Trending Main Engine Assembly (MEA) Cover Actuator Performance using Cassini Attitude Control Flight Data

Luis G. Andrade Jr.*
Jet Propulsion Laboratory, California Institute of Technology, Pasadena, CA, 91109

This paper proposes two different methods of estimating the disturbance torque imparted on the Cassini spacecraft by its Main Engine Assembly (MEA) cover actuator, using attitude control flight data. The Cassini spacecraft is a long-lived orbiter that has spent over 18 years in space at the time of writing this paper. With any spacecraft in operation that long, the operations team must attempt to anticipate a system failure as early as possible. The Cassini spacecraft has an actuation mechanism that opens and closes an accordion-like cover that protects its MEA from space debris. With almost 80 full actuation cycles done on the MEA cover actuator, and more planned for the remainder of the mission, this study will attempt to trend the performance of the MEA cover actuator mechanism throughout the course of the mission. This study explores methods of trending the performance of actuation mechanisms when direct actuator torque measurements are not available, and when flight data is a limited resource, in an attempt to gain insight into the status of the Cassini MEA cover actuator.

Acronyms

AACS	=	Cassini Attitude and Articulation Control Subsystem
ASI	=	Italian Space Agency
CM	=	Center of mass
DDA	=	Dual Drive Actuator
ESA	=	European Space Agency
EGA	=	Engine Gimbal Assembly
FOM	=	Figure of Merit
FSDS	=	Flight Software Dynamic Simulation
FSW	=	Flight Software
HGA	=	High Gain Antenna
MEA	=	Main Engine Assembly
MOI	=	Moment of inertia
MMH	=	Monomethylhydrazine
NASA	=	National Aeronautics and Space Administration
NTO	=	Nitrogen Tetroxide
OTM	=	Orbit Trim Maneuver
PDT	=	Pacific Daylight Time
POI	=	Product of inertia
RCS	=	Reaction Control Subsystem
REU	=	Remote Engineering Unit
RWA	=	Reaction Wheel Assembly
RWAC	=	Reaction Wheel Attitude Controller
S/C	=	Spacecraft
SCO	=	Cassini Spacecraft Operation Team
SOI	=	Saturn Orbit Insertion
TCM	=	Trajectory Correction Maneuver
T/D	=	Cassini Thermal/Devices Subsystem

* Cassini Attitude Control Operations Engineer, Guidance and Control Section, M/S 230-104, 4800 Oak Grove Dr., Pasadena, California, 91109, Luis.G.Andrade@jpl.nasa.gov

I. Introduction – Cassini Mission to Saturn

A. Overview of Cassini Mission

THE Cassini-Huygens mission is a collaborative effort between the National Aeronautics and Space Administration (NASA), the European Space Agency (ESA), and the Italian Space Agency (ASI). Cassini-Huygens was launched in October 1997 onboard a Titan IVB/Centaur, and followed a "VVEJGA" trajectory, using gravity assists from two Venus flybys, one Earth flyby, and one Jupiter flyby before arriving at Saturn. The spacecraft entered Saturn's orbit on July 1, 2004 PDT after travelling a total distance of 3.5 billion km (about 2.2 billion mi). Once in Saturn's orbit, the Cassini spacecraft deployed the 320 kg ESA-built Huygens probe into the atmosphere of the moon Titan before beginning its study of the Saturnian system via its diverse suite of "remote sensing" and "direct sensing" instruments. At the time of writing this paper, Cassini has spent over 18 years in space, 11 of those years being spent conducting demanding science campaigns that have taken their toll on different spacecraft subsystems. The Cassini program is currently in its second extended mission, which is slated to end in September of 2017. At the end of its second extended mission, Cassini will be purposely flown into the harsh atmosphere of Saturn, at which point it will send back to earth never-before-collected science data before the Saturnian atmosphere destroys the orbiter. At the end of its life, Cassini will have accumulated nearly 20 years of spaceflight, along with the associated "wear and tear" to its onboard systems.

B. Motivation and Objectives of this Study

To operate a spacecraft such as Cassini, for almost 20 years, the Spacecraft Operations (SCO) team must meticulously monitor the spacecraft's "consumables", which include items such as monopropellant and bipropellant levels. Similarly, the SCO team must make a proactive attempt to foresee a failure or detect degradation in any of the spacecraft subsystems, by monitoring the spacecraft "vital signs". Similar to how a physician might attempt to diagnose the early onset of disease in a patient, so to must a spacecraft operations team look for signs that the spacecraft might be degrading in some respect. On Cassini, "vital signs" that are monitored include Reaction Wheel Assembly (RWA) bearing drag torque, thrust degradation in the Reaction Control Subsystem (RCS) thrusters, and excessive subsystem power draw.

In all spacecraft with continually actuating mechanisms, including Cassini, degradation and failure is always a concern as a faulty actuator mechanism can severally limit a mission or even end it. One important actuation mechanism on Cassini that is carefully tracked is the actuator that opens and closes the Main Engine Assembly (MEA) cover. This cover is an accordion-like mechanism that shields the MEA from micro-meteoroid and orbital debris impacts throughout the span of the mission, but must be open prior to MEA firings. The MEA cover actuator has been closed/opened almost 80 times since 1997, and continues to be actuated. Since launch, the SCO Thermal/Devices (T/D) team has documented the number of actuations of the MEA cover, and has trended the achieved cover angle at the end of each actuation. The SCO T/D team also monitors temperature and current loads from the MEA cover actuator. However, to date, no attempt has been made to characterize the performance of the MEA cover actuator using attitude control flight data. An attitude control flight data analysis on the performance of the MEA cover actuator is valuable to the SCO team, as it serves as an additional diagnostic tool to determine the health of the MEA cover actuation system.

The Cassini project staff is currently involved in the design of the "Proximal Orbits", the final phase of Cassini's mission. In its final phase, Cassini will fly 22 orbits between the innermost D-ring and the top of Saturn's atmosphere.[1] The D-ring is diffuse, and it is not certain how far down towards Saturn's cloud tops the D-ring particles reach. Current ring models suggest there is low likelihood of Cassini impacting D-ring particles during the Proximal Orbits, as they are currently designed, but in-situ measurements (never collected before) of the innermost region of the D-rings during Proximal Orbits may indicate otherwise. Still, the Proximal Orbit crossings near the D-ring are the most dangerous faint ring crossings in the entire mission, with particles travelling at velocities exceeding 30 km/s relative to Cassini.[1]

Although the project plans on flying the spacecraft through an area with low likelihood of impact with high-speed ring particles, safety measures are still taken to protect the spacecraft from unforeseen impacts. One safety measure is to point the High Gain Antenna (HGA) on Cassini into the direction of oncoming flow, effectively using the HGA parabolic dish as a shield for the rest of the orbiter.[1] Another safety measure is to close the MEA cover over the MEA during these last 22 proximal orbits, and only open the cover if there is a need for an MEA Orbit Trim Maneuver (OTM). If the MEA cover actuator fails in a partially-closed partially-open position, it would jeopardize both the protection of the MEA from oncoming particles as well as the safe execution of an MEA OTM, whose thrust plume would be infringed upon by the partially closed cover.

The Proximal Orbits phase is not the only time the MEA cover actuator will be used. The spacecraft currently flies through other areas of Saturn's ring plane that also pose a "dust hazard" to the spacecraft. To protect the MEA, the cover is closed over the engine when crossing a dust hazard, and it is opened back up before the next MEA OTM.[2]

Since the MEA cover has been actuated for nearly 80 cycles, much longer than the originally intended 20-cycle lifespan, and will continue to be actuated until the end of mission, it is important to use all available methods of trending the performance of the cover mechanism.[2] The purpose of this paper is to present two methods of trending the performance of the MEA cover actuator using SCO Attitude and Articulation Control Subsystem (AACS) flight data over a selection of MEA cover actuation events from 2004 until 2015. During these cover actuations, the spacecraft was in RWA control, and commanded to an inertially fixed attitude. Ideally, the performance of the MEA cover mechanism would be evaluated by measuring actuator output torque. However, actuator torque is not observable via telemetry. Nevertheless, as part of the regular set of AACS telemetry, certain flight data is included that can be used to estimate the "disturbance" torque imparted by the rotating MEA cover on the spacecraft. Trending MEA cover disturbance torque over the course of the mission may reveal unexpected changes in the torque time history, which could be associated with degradation of the MEA cover actuation mechanism. Identifying degradation of the cover actuator would give the SCO team an early warning of potential failure.

C. Challenges Faced in the Trending of Actuator Torque

In the process of carrying out this study, three fundamental challenges were faced, which shaped the approach taken in trending the MEA cover actuations.

1. *An inability to directly measure actuator torque.* On the Cassini spacecraft, bearing torque from the RWAs is estimated onboard by a local PI controller[3] and sent down to the ground as flight data. However, no such flight data is produced for the torque of the MEA cover actuator. To compensate for this, the *disturbance* torque imparted on the S/C during cover actuations is calculated as an indirect method of trending MEA cover actuator torque.
2. *An unknown "true" disturbance torque profile.* Ideally, estimated disturbance torques from flight data would be compared against a baseline predicted torque profile, derived from a model of the spacecraft (S/C) dynamic response to the MEA cover actuation. However, this "true" disturbance torque profile was not available for this study. To compensate for this, two different methods of torque profile estimation, using different sources of flight data were developed. Estimating disturbance torque using two different reconstruction methods allows a comparison and validation of both methods.
3. *A sparsity of available flight data.* Due to a limited telemetry bandwidth, and competing telemetry channels, limitations are placed on the sampling rate of different telemetry channels. Consequently, the flight data available for each MEA cover actuation is sparse. From AACS flight data, spacecraft body rate data is sampled at ¼ Hz frequency, RWA rate data is sampled at ¼ Hz frequency, and attitude control error (position error) data is sampled at ½ Hz frequency. The T/D subsystem has dedicated telemetry channels that provide information about the MEA cover mechanism, although not an actuator torque measurement. However, the T/D flight data is sampled at 1/64 Hz frequency (once every 64 seconds). To compensate for the sparsity of AACS flight data, smoothing and interpolating techniques are employed.

II. The Cassini Spacecraft

Cassini is a 3-axis stabilized spacecraft[4] with an 11-meter magnetometer boom and three 10-meter Radio and Plasma Wave Science (RPWS) antennas (Fig. 1). Cassini has a body-fixed 4-meter diameter HGA parabolic reflector dish for telecommunications. At launch, the total spacecraft mass was 5,560 kg of which 3,000 kg was liquid bi-propellant and 132 kg was hydrazine.

A. The Reaction Control Subsystem (RCS)

The Cassini orbiter is equipped with two separate systems that can be used for delta-V events, including OTMs, Trajectory Correction Maneuvers (TCMs), and unique events such as Saturn Orbit Insertion (SOI). The RCS system, composed of 4 hydrazine thrusters along the ±Y-axes and 4 hydrazine thrusters along the –Z-axis, is used for relatively small delta-V maneuvers where the magnitude of the desired delta-V is less than 300 mm/s. When the spacecraft is performing a delta-V maneuver with the RCS system, only the 4 Z-facing thrusters contribute to the delta-V.[5,6]

In addition to delta-V maneuvers less than 300 mm/s in magnitude, the RCS system also doubles as one of two attitude control systems.[4] When the spacecraft is under RCS attitude control, onboard flight software off-pulses all eight active RCS thrusters (Fig. 2). The 4 thrusters along the ±Y-axes fire as couples (Y1-Y3 fire as one pair, and Y2-Y4 fire as another pair). Assuming both thrusters in a pair are balanced with each other, a Y-thruster pair fires without imposing a net delta-V on the spacecraft. Rather, a Y-thruster pair provides a purely rotational control torque about the Z-axis. The 4 thrusters pointing along the –Z-axis fire independently of each other and are used for X and Y-axis rotational control. When any of the 4 Z-facing thrusters fire, they impart both a net delta-V and a control torque on the spacecraft.[5,6]

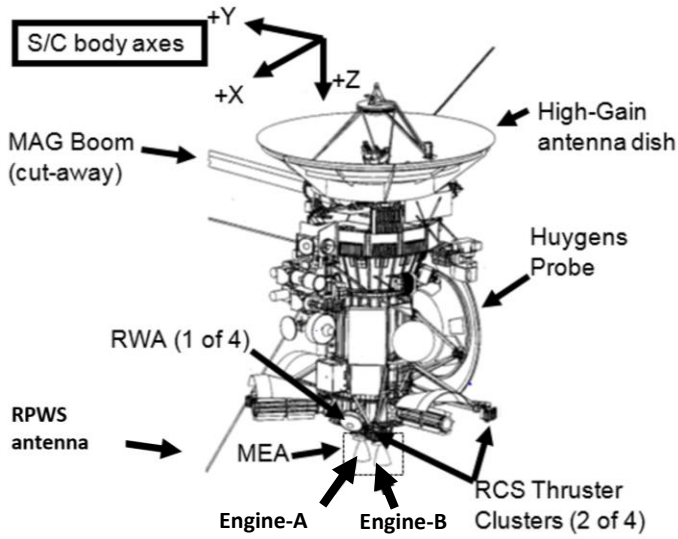

Figure 1. Overview of Cassini spacecraft.

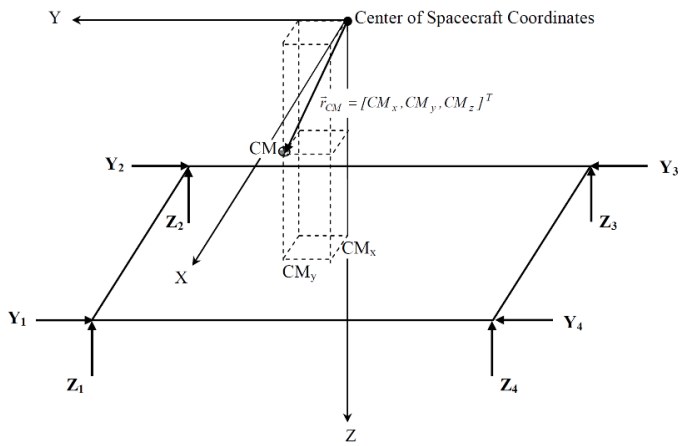

Figure 2. Thruster layout of reaction control subsystem on Cassini.

B. The Main Engine Assembly (MEA) and the MEA Cover Design

The second system on the Cassini orbiter that is used for delta-V maneuvers is the MEA. The MEA, composed of 1 active rocket engine and 1 backup rocket engine, using a hypergolic bi-propellant combination of monomethylhydrazine (MMH) and nitrogen tetroxide (NTO), is used for orbital trim maneuvers with delta-V magnitudes greater than 300 mm/s. The spacecraft's MEA contains two rocket engines mounted side-by-side at the end of the spacecraft opposite the HGA; Engine-A is set as prime, and Engine-B is set as backup (Fig. 1). Only Engine-A has been fired, and the unused Engine-B serves only for redundancy. Each of the engines has a dedicated Engine Gimbal Assembly (EGA), which provides 2-axis control of its respective engine nozzle using two linear engine gimbal actuators.[2] During an MEA burn, the EGA provides control about the X and Y spacecraft axes, while the RCS system provides roll control about the Z spacecraft axis, i.e. the axis of the MEA thrust vector. See Fig. 1 for the layout of the Cassini orbiter, including hardware location relative to spacecraft axes.

The MEA cover is a semi-flexible accordion-like shield that extends over both Engine-A and Engine-B in its "deployed" (closed cover) configuration, and retracts back over both engines in its "stowed" (opened cover) configuration. It is necessary to deploy the MEA cover over both engines during events where the engines can be damaged by hypervelocity impacts with micrometeoroids and orbital debris[2]; one such event is referred to as a "dust hazard". For ring plane crossings that pose a dust hazard to the spacecraft, the MEA cover is deployed, and after the spacecraft is clear of dust particles, the MEA cover is stowed, so that the main engine can once again be fired without the cover infringing into the path of the engine plume.

The Cassini MEA cover is actuated open or closed by commanding a rotational Dual Drive Actuator (DDA), composed of two brushless DC motors denoted as motor-A and motor-B.[7] The DDA is an electromechanical actuator that was originally developed for the NASA-JPL Galileo spacecraft, and later adapted for the Space Shuttle's Spaceborne Imaging Radar-C.[8,9] The DDA offers redundancy by providing two independent drive trains that combine at a common output shaft which is attached to the Cassini MEA cover.[9] For any actuation of the cover, both or either motor can be used. The angle of the MEA cover can be measured using a potentiometer mounted along the axis of rotation of the DDA (parallel to the ±Y-axis).[2] At the end of any stow actuation, telemetry from the potentiometer is used to verify the cover is sufficiently open, and not infringing into the path of the main engine exhaust. Likewise, potentiometer telemetry is used at the end of a deploy actuation to verify the cover is fully closed over the main engine.

The DDA has two microswitches along its axis of rotation. One switch is tripped when the cover is deployed; the other switch is tripped when the cover is stowed.[2] When the cover is in between stowed and deployed positions, the microswitches report the cover is neither stowed nor deployed. In the case that the potentiometer and the microswitches report a cover failure in the deployed, or partially stowed position, pyrotechnic bolt cutters can be used to permanently jettison the MEA cover.[2] However, as in any spacecraft, especially one that has endured close to 20 years of space flight, firing the pyros to jettison the MEA cover poses a high operational risk, and is considered a "last resort" option.

Figure 3, shows diagrams of the MEA cover in stowed/deployed configuration, looking along both the ±Y axis. Note that because both Engine-A and Engine-B are co-aligned with each other, along the axis of rotation of the DDA (parallel to Y-axis), depending on whether one is looking along the +Y or –Y-axis, either Engine-A or Engine-B will be visible, but not both. The diagrams in Fig. 4 are simplified representations of the actual MEA, and are not drawn to scale. Their purpose is to depict the relative stow/deploy motion of the cover, and the location of the DDA and potentiometer. The reader is referred to Appendix A for additional diagrams and images of the Cassini MEA cover assembly.

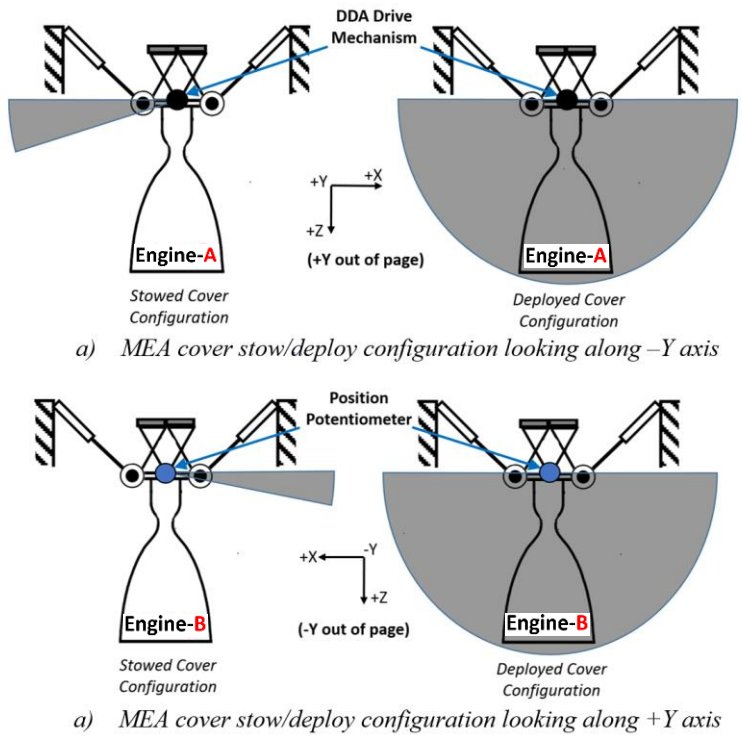

Figure 3. MEA cover, DDA location, and potentiometer location.

The MEA cover assembly was originally designed with a 20-cycle in-flight consumable limit in mind.[2] Each complete cycle consists of fully *deploying* the cover to ~180° and *stowing* it back to the minimum angle allowed by the stiffness of the folded MEA cover (~33°). The 20-cycle in-flight limit was meant to span from launch in 1997 to SOI in July of 2004.[2] Since SOI, until now, Cassini has needed to cycle its MEA cover approximately 60 more times, mostly for MEA OTMs and dust hazards. In light of the fact that the MEA cover has greatly exceeded its original 20-cycle in-flight consumable limit, and keeping in mind that there will be several more MEA cover actuations between the time of writing this conference paper and the end of Cassini's Solstice Mission in September 2017, the SCO team would benefit from an analysis of the state of the MEA cover actuation mechanism.

Since launch, all but two MEA cover actuations were performed only using motor-A in the DDA. For this reason, the analysis in this paper is focused on evaluating the health of motor-A, not motor-B which up until now has served as a backup motor in the DDA. Furthermore, data from both deployment and stow actuations is analyzed in this study, but the body of the paper focuses only the deployment data, which was found to contain a trendable signature that suited the purpose of this paper. The stow actuation data exhibited a much less clear trend to extract. Analyzed stow data is included in Appendix B for the reader's reference. The AACS torque reconstruction methods in this paper will be illustrated using data from a recent MEA cover deployment activity that occurred on September 29, 2015.

C. The Cassini Spacecraft Reaction Wheel Control System

Although the RCS control subsystem has certain benefits over the RWA control subsystem, most notably, its greater control authority, Cassini spends the majority of its time in RWA control. Flying under RWA control is almost always preferred because it improves pointing accuracy and stability, and also conserves hydrazine usage. This study deals with MEA cover actuations that took place while Cassini was in RWA control in a "quiescent" state (pointing at an inertially fixed attitude). The disturbance torques imparted on the spacecraft during an MEA cover actuation are weak enough that the RWA control subsystem can safely absorb them. In the remainder of this section, certain aspects of the design of the Reaction Wheel Attitude Controller (RWAC) will be discussed, as they pertain to this paper.

The Cassini spacecraft is equipped with a total of 4 Reaction Wheel Assemblies (RWAs). At launch, RWA-1, 2, and 3, where set as the prime RWAs and were aligned orthogonal to each other and equidistance from the S/C Z-axis. RWA-4 was designed as a backup should any of the three primary wheels fail. RWA-4 is mounted on a platform that can be articulated to the position of any of the three primary wheels. At launch, RWA-4 was positioned parallel to RWA-1 and was set as backup. On July 11, 2003, RWA-4 was articulated to the position of RWA-3 after the RWA-3 bearings began exhibiting troublesome behavior. To date, the prime wheels are RWA-1, RWA-2, and RWA-4, with the troublesome RWA-3 now taking the role of backup.

Figure 5 shows the conceptual block diagram of the Cassini Reaction Wheel Attitude Controller (RWAC). The basic structure of the RWAC algorithm is a decoupled, three-axis Proportional and Derivative controller.[3] Due to the presence of bearing frictional torque in the RWAs, the "PD" design of the RWAC is unable to drive the spacecraft attitude control error to zero. To remedy this, the RWA hardware manager module on Cassini was modified to include friction estimation and compensation through the use of a "local" (Proportional + Integral) estimator.[3]

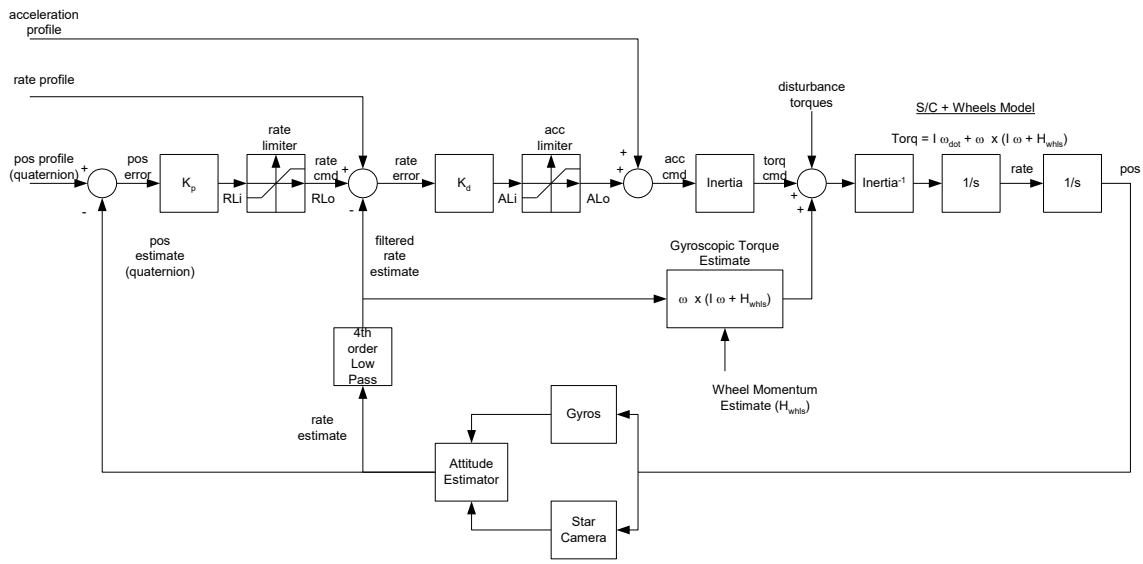

Figure 4. Conceptual block diagram of the Cassini RWAC.[3]

The control torque being output by the RWAC algorithm is determined by Eq. (1):

$$Control\ Torque = I_{SC}\frac{d\omega}{dt} + \omega \times (I_{SC}\omega + H_{RWA}) \tag{1}$$

where, ω is the spacecraft angular rate vector in body-fixed coordinate frame. H_{RWA} is the total angular momentum vector of the three prime reaction wheels in body-fixed coordinate frame. I_{SC} is the inertia tensor of the entire orbiter, and $\frac{d\omega}{dt}$ is the spacecraft angular acceleration.[10]

The RWAC algorithm works together with the *Attitude Commander* module and the *Attitude Estimator* module. The Attitude Commander generates a commanded or "profiled" position in quaternion form, a profiled rate, and a profiled acceleration. The Attitude Estimator uses data from the onboard gyroscope and Star Tracker, denoted as "Star Camera" in the diagram, to generate the current position and body rates of the spacecraft. The position and rate estimate that is output by the Attitude Estimator is used to calculate the "position error" and "rate error" which the RWAC algorithm aims to minimize using its Proportional and Derivative gains.[3] Before the Attitude Estimator's rate estimate is subtracted from the total commanded rate in the feedforward path of the RWAC algorithm, it first passes through a 4th order low-pass filter. The 4th order low-pass filter serves to remove any signal content related to high frequency magnetometer boom oscillations, which can be destabilizing to the control loop.[3]

III. Estimation of MEA Cover Disturbance Torque using RWA Flight Data

The primary method AACS has developed to reconstruct the torque profile of motor-A in the MEA cover Dual Drive Actuator (DDA) relies on the principle of angular momentum conservation. During MEA cover actuations (deploy and stow), the spacecraft is commanded to maintain a quiescent attitude in an inertial frame. In order for the

spacecraft to maintain the commanded quiescent attitude, the angular momentum imparted on Cassini due to the DDA time-varying torque must be absorbed by the RWAs. Therefore, it is expected that flight data will show a change in RWA rates during the MEA cover actuation. Figure 5 shows raw (unmodified) RWA rate flight data for the MEA cover deployment that took place on September 29, 2015. Since the inertia of the MEA cover assembly is so small compared to the inertia of the complete spacecraft[†], the actuation of the cover produces only a faint, but noticeable, change in each wheel's rate, on the order of 10 rpm per RWA. Note that RWA rates from flight data are originally in rad/sec, but are converted to RPM for Fig. 5. It's also important to note that because Cassini is an isolated system during an MEA cover actuation (no external torques applied to the spacecraft) the RWA rates return to their original value at the end of the cover actuation.

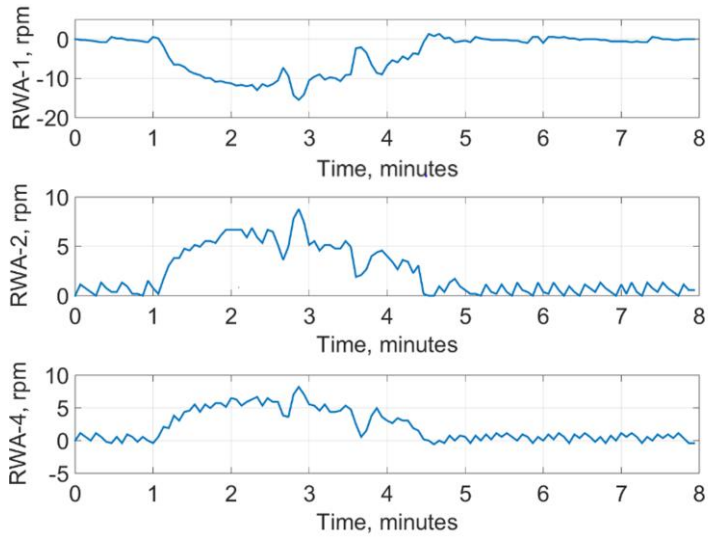

Figure 5. Raw RWA rate flight data. *This figure shows the accumulated RWA rate data for the cover deployment activity on September 29, 2015. The net accumulated RWA rates at the end of the cover deployment returns to zero because the spacecraft is an isolated system during the MEA cover deployment.*

A. Mathematical Derivation of "RWA Momentum" Method of Torque Reconstruction

The total accumulated angular momentum in the closed spacecraft system during cover actuation is a function of the spacecraft momentum, $\vec{H}_{SC}$, and the RWA momentum, $\vec{H}_{RWA}$. It is expressed in Eq. (2).

$$\vec{H}_{Total} = \vec{H}_{SC} + \vec{H}_{RWA} \tag{2}$$

The spacecraft momentum, $\vec{H}_{SC}$, is a function of the *effective* inertia tensor of the spacecraft, I_{SC}, and the body rate vector, $\vec{\omega}$, and their relationship is given in Eq. (3).

$$\vec{H}_{SC} = I_{SC}\vec{\omega} = \begin{bmatrix} I_{XX} & I_{XY} & I_{XZ} \\ I_{YX} & I_{YY} & I_{YZ} \\ I_{ZX} & I_{ZY} & I_{ZZ} \end{bmatrix} \begin{bmatrix} \omega_x(t) \\ \omega_y(t) \\ \omega_z(t) \end{bmatrix} \tag{3}$$

The *effective* inertia tensor takes into account the fact that during a cover actuation, the spacecraft behaves as a two-body system composed of the "spacecraft without the cover" and the "MEA cover" joined together at the axis of rotation of the DDA. The effective inertia tensor subtracts the inertial properties of the MEA cover. On Cassini, the largest product of inertia (POI) is only 3.6% of the smallest moment of inertia (MOI), so it is a reasonable simplification to assume all POIs are zero.[10] The *effective* MOIs of Cassini are estimated using the *parallel-axis*

[†] The MEA cover's Y-axis MOI, I_{YY}^{cover}, is ~5.8 kg-m^2, relative to the local cover CM, while the total S/C Y-axis MOI, $I_{YY}^{SC+cover}$, is ~5,333 kg-m^2 relative to the S/C global CM. The perpendicular distance between the S/C global Y-axis and the local cover Y-axis is ~2.44 m. After solving for I_{YY}^{cover} relative to the global S/C CM, it is determined that the Y-axis MOI of the cover is ~2% of the Y-axis MOI of the complete S/C.

theorem as shown in Eq. (4). In Eq. (4), $I_{XX}^{SC+cover}$, $I_{YY}^{SC+cover}$, and $I_{ZZ}^{SC+cover}$ are the MOIs about the primary spacecraft body axis of the *total* spacecraft/cover system. The variables I_{xx}^{cover}, I_{yy}^{cover}, I_{zz}^{cover}, and m_{cover} are the estimated MOIs of the standalone MEA cover and its mass. The position vector, $\vec{L}$, of the MEA cover center of mass, $\overrightarrow{CM_{cover}}$, relative to the spacecraft center of mass, $\overrightarrow{CM_{SC}}$, is given by Eq. (5). Note that the inertia tensor of the spacecraft varies with time as fuel is consumed, and the mass distribution changes.

$$I_{XX} = I_{XX}^{SC+cover} - \left\{I_{xx}^{cover} + m_{cover}(L_y^2 + L_z^2)\right\} \tag{4.a}$$
$$I_{YY} = I_{YY}^{SC+cover} - \left\{I_{yy}^{cover} + m_{cover}(L_x^2 + L_z^2)\right\} \tag{4.b}$$
$$I_{ZZ} = I_{ZZ}^{SC+cover} - \left\{I_{zz}^{cover} + m_{cover}(L_x^2 + L_y^2)\right\} \tag{4.c}$$

$$\vec{L} = \left[L_x\ L_y\ L_z\right] = \overrightarrow{CM_{cover}} - \overrightarrow{CM_{SC}} \tag{5}$$

The spacecraft body rate vector, $\vec{\omega}$, needed for the computation of $\vec{H}_{SC}$ is obtained from flight data sampled once every 4 seconds, or at a sampling frequency of ¼ Hz. Figure 6 shows the raw spacecraft body rate flight data, typical of all MEA cover actuations analyzed in this study. The body rates about each axis are zero, which is consistent with the fact that the spacecraft is commanded to an inertially quiescent attitude during MEA cover actuations. The noisy signals present in the body rate data are due to noise in the onboard gyroscopes. Therefore, it is reasonable to assume body rates are equal to zero.

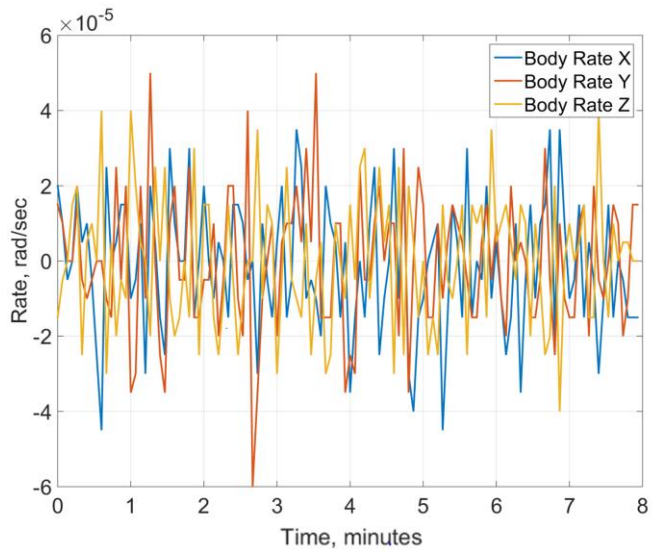

Figure 6. Raw body rate flight data. *This figure shows S/C body rate data is effectively zero for the deploy activity on September 29, 2015.*

Assuming the spacecraft body rate vector, $\vec{\omega}$, is zero simplifies the momentum balance expression of Eq. (2) to the expression shown in Eq. (6). From Eq. (6), it can be assumed that the total accumulated angular momentum due to an MEA cover actuation is fully captured in the accumulation of angular momentum of the RWAs.

$$\vec{H}_{Total} \approx \vec{H}_{RWA} \tag{6}$$

The accumulated angular momentum absorbed by the RWAs is a function of the RWA rates, $\vec{\rho}$, given by the flight data in Fig. 5[‡]. The MOI of each wheel about its spin axis is well known, and is constant over time. The MOIs of the active RWAs are placed into a diagonal matrix, I_{RWA}. A coordinate transformation matrix, T, is used to transform the angular momentum from the RWA coordinate system, to the spacecraft body frame. The calculation of accumulated angular momentum is given in Eq. (7).

[‡] The accumulated angular momentum is calculated with RWA rates in units of rad/s

$$\vec{H}_{rwa} = TI_{RWA}\vec{\rho} = \begin{bmatrix} 0 & \frac{-1}{\sqrt{2}} & \frac{1}{\sqrt{2}} \\ \sqrt{\frac{2}{3}} & \frac{-1}{\sqrt{6}} & \frac{-1}{\sqrt{6}} \\ \frac{1}{\sqrt{3}} & \frac{1}{\sqrt{3}} & \frac{1}{\sqrt{3}} \end{bmatrix} \begin{bmatrix} I_{RWA-1} & 0 & 0 \\ 0 & I_{RWA-2} & 0 \\ 0 & 0 & I_{RWA-4} \end{bmatrix} \begin{bmatrix} \rho_{rwa-1} \\ \rho_{rwa-2} \\ \rho_{rwa-4} \end{bmatrix} \tag{7}$$

The resulting $\vec{H}_{RWA}$ from Eq. (7) is in the spacecraft body frame and provides a momentum calculation once every 4 seconds, at the same interval as the RWA rate data. Cubic spline interpolation is used to obtain momentum estimates once every second. Once $\vec{H}_{RWA}$ has been interpolated to a 1-second interval, the momentum data is smoothed using weighted linear least squares and a 2nd degree polynomial model. Figure 7 shows the smoothed accumulated momentum curves about each body axis. The smoothing technique can be tuned by adjusting the *span* of samples that the technique uses to calculate a smoothed momentum sample. Presently, the span has been tuned to be 8% of the total number of samples in an actuation activity. The method used to tune the smoothing technique will be discussed in a section VI-A. From Fig.7, it is seen that the accumulation of angular momentum occurs about the spacecraft's Y-axis, with approximately zero angular momentum being accumulated in the X or Z-axes. This result is expected, since the rotation axis of the MEA cover (torque vector of motor-A) is pointed parallel to the ±Y-axis. Refer to Fig. 3 for a visual representation of the movement of the MEA cover. Note from Fig. 7, that at the end of the deployment activity, the Y-axis accumulated angular momentum returns to zero because no net external torques are applied to the spacecraft. The momentum accumulated by the spacecraft is a result of the MEA cover motion, and returns to zero once the cover comes to a stop.

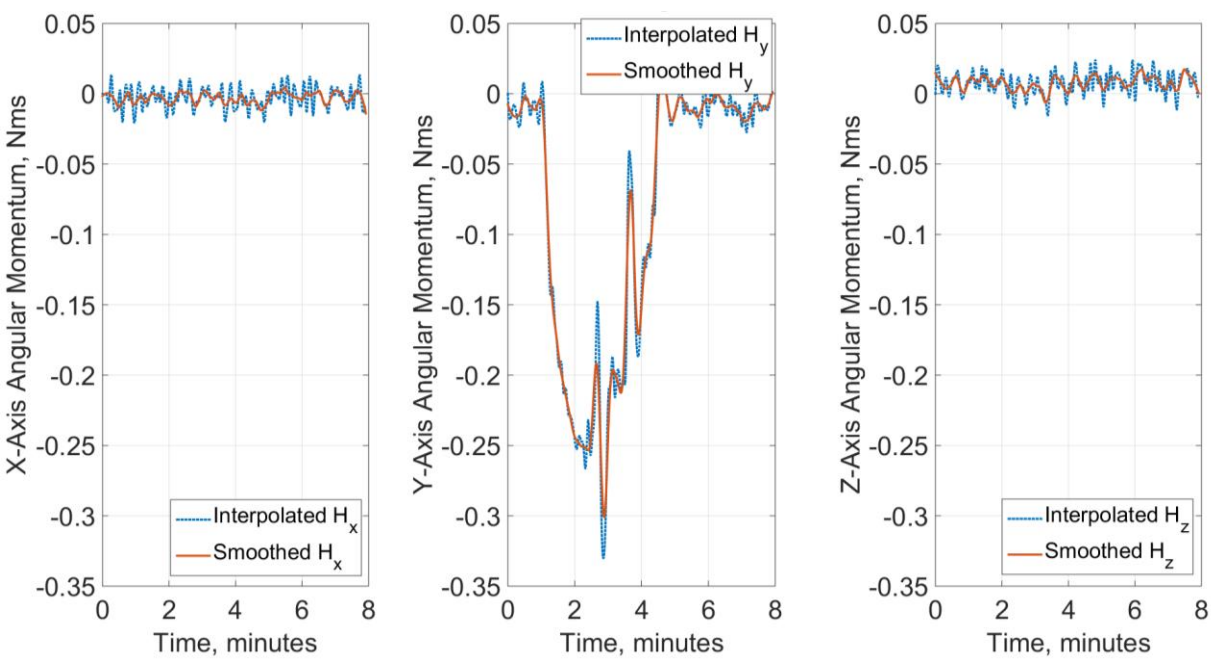

Figure 7. Smoothed accumulated angular momentum. *This figure shows a comparison of the interpolated angular momentum curves before being smoothed (blue) and after being smoothed (orange) for the MEA cover deployment activity on September 29, 2015. The resulting momentum is expressed in the spacecraft body frame.*

Since the accumulated angular momentum resulting from the MEA cover actuations is only present about the spacecraft Y-axis, the disturbance torque of motor-A, T_{total_y}, can be calculated by taking the time derivative of the Y-axis angular momentum. This conclusion is expressed in Eq. (8).

$$T_{total_x} = \frac{dH_{total_x}}{dt} \approx 0 \tag{8.a}$$

$$T_{total_y} = \frac{dH_{total_y}}{dt} \neq 0 \tag{8.b}$$

$$T_{total_z} = \frac{dH_{total_z}}{dt} \approx 0 \tag{8.c}$$

Consequently, the primary method AACS has developed to reconstruct the disturbance torque profile of motor-A in the MEA cover Dual Drive Actuator (DDA) is henceforth denoted as $T_{H_{rwa}}$ and is expressed by Eq. (9).

$$T_{H_{rwa}}(t) = T_{total_y}(t) \tag{9}$$

B. Results of "RWA Momentum" Method of Torque Reconstruction

Using Eq. (9), the torque profile proposed by the primary AACS method of reconstruction, is shown in Fig. 8. As discussed in section I-C, the Cassini team does not have a *predicted* or *true* torque profile to which the reconstructed torque profile of Fig. 8 can be compared against. The lack of visibility into the friction and flexibility of the MEA cover structure makes it difficult to identify the physics of what is occurring during the actuation. However, one thing that can be done is to compare the torque time history derived from RWA momentum, to the T/D subsystem data collected during the same actuation activity. Recall that the T/D data is collected in intervals of 64 seconds. This sparsity of data makes it difficult to know what is going on in between samples. Figure 9 presents the set of T/D data for the same MEA cover deployment in Fig. 8. All MEA cover actuations (deploy/stow) are commanded in the same way. At minute "1", motor-A in the DDA is commanded on (polarity depends on whether activity is deploy or stow). At minute "7", motor-A is commanded off. The cover actuation is an open-loop process, which means that motor-A turns off after a pre-set run time regardless of the cover angle. The cover reaches its final angle in ~3 min, and 3 more minutes is added to the commanded motor run time for padding (6 min total). Once motor-A is turned off, the DDA holds its final position. From Fig. 9, it is seen that there is a large jump in motor-A's current draw between the data point before minute "4" and the data point immediately after minute "4". Also, Fig. 9 shows that the MEA cover position keeps increasing, starting at the "stowed" position of 32.75° and ending at the "deployed" position of 179.2°. The potentiometer reports that 179.2° is reached at the same time as the jump in current, at minute "4.27". These two coinciding sources of flight data suggest that the deployment activity that started at minute 1, actually reaches full deployment (hits hardstop) at minute "4.27". At this point, motor-A stalls until minute "7" when the pre-set 6 minute run time finishes. The point of stall, denoted by the green dotted line in Figs. 8 and 9, also coincides with the start of a torque excursion in Fig. 8. After the torque excursion at minute "4.27", the torque profile winds down and dwells at approximately zero for the remainder of the deployment activity. It is observed that the torque profile computed in Fig. 8 is excited beginning at minute "1", coinciding with the command to turn on motor-A, and begins settling down after minute "4.27", the point at which the deployment has completed (cover stops moving) and the motor stalls.

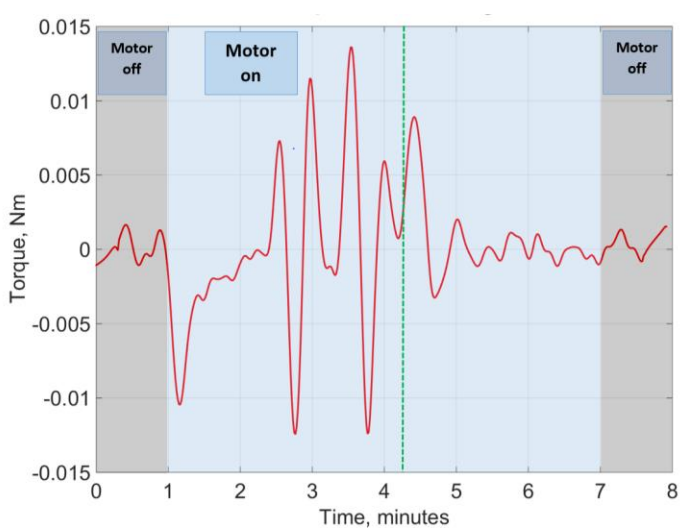

Figure 8. Disturbance torque imparted by motor-A and derived from Y-axis RWA momentum. *$T_{H_{rwa}}$ for deploy activity on September 29, 2015. Green line denotes point at which the cover reaches full deployment, and when motor-A stalls.*

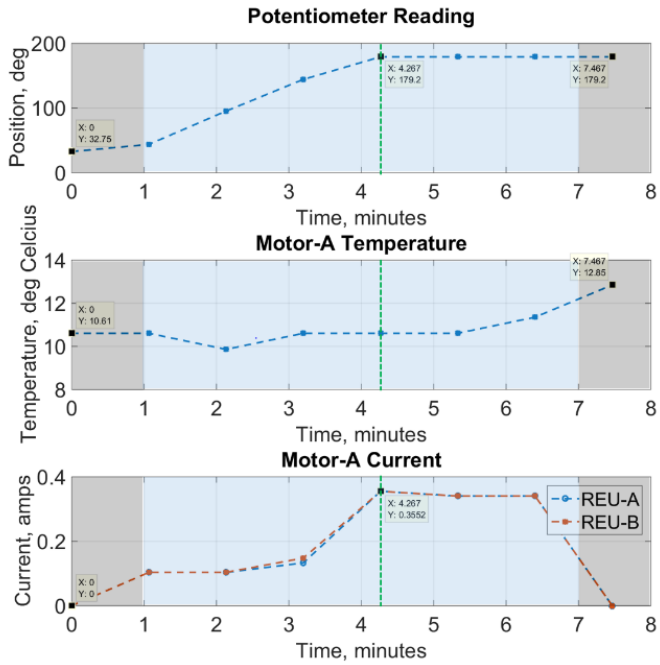

Figure 9. Motor-A Thermal/Devices data. *Position, temperature, and motor current data for MEA cover deployment activity on September 29, 2015. Green line denotes point at which the cover reaches full deployment, and when motor-A stalls. Remote Engineering Units (REUs) A and B sample basic hardware engineering data including voltages, currents, and potentiometer measurements.*

IV. Estimation of MEA Cover Disturbance Torque using Position Error Flight Data

Since a model of the expected dynamic response to the MEA cover actuator disturbance torque is not available, a second method of reconstructing the torque profile must be used, to verify whether the primary method of reconstructing torque (using RWA accumulated momentum) is correct.

The Cassini AACS team has previously done work to develop various methods of estimating disturbance torque imparted on the spacecraft during low Enceladus flybys, where the spacecraft flies through plumes ejected from the moon's south polar region. In these flybys, the plumes of Enceladus impart an *external* disturbance torque on the spacecraft that needs to be countered by the attitude control system, either by firing RCS thrusters, or by absorbing the externally accumulated momentum with the RWAs. This work is found in Ref. 10 and 11, and in section IV-A one of these methods is adapted to suit the purpose of estimating MEA cover disturbance torque.

A. Mathematical Derivation of "Transfer Function" Method of Torque Reconstruction

Figure 4 shows the conceptual block diagram for the RWAC algorithm, the attitude controller that uses RWAs. From the RWAC controller, let the commanded attitude be $\theta_C(s)$, the commanded rate be $\omega_C(s)$, and the commanded acceleration be $\alpha_C(s)$. Let the disturbance torque the spacecraft is subjected to by an MEA cover actuation be denoted as $T_D(s)$, let the gyroscopic torque from the RWAs be denoted as $T_{gyro}(s)$ and let the resulting attitude control error (also called position error) be denoted by $e_\theta(s)$. From Fig. 4, the resulting spacecraft attitude $\theta(s)$ can be expressed in the Laplace domain by Eq. (10).[10]

$$\theta(s) = G_\theta(s)\theta_C(s) + G_\omega(s)\omega_C(s) + G_\alpha(s)\alpha_C(s) + G_T(s)[T_D(s) + T_{gyro}(s)] \tag{10}$$

In Eq. (10), the various "$G(s)$" terms represent transfer functions from the various stimuli, such as disturbance torque, to spacecraft attitude. Recalling that the MEA cover actuations occur at a quiescent attitude, Eq. (10) can be simplified by setting $\theta_C = \omega_C = \alpha_C = 0$. Furthermore, since $\omega_C = 0$ then $T_{gyro} = 0$. From Ref. 10, the transfer function between the disturbance torque, $T_D(s)$, and the attitude control error, $e_\theta(s)$ is given by Eq. (11).

$$\frac{e_\theta(s)}{T_D(s)} = -\frac{(s^2+2\zeta\omega s+\omega^2)^2/I_{SC}}{Den(s)} \tag{11.a}$$

$$Den(s) = s^6 + 4\zeta\omega s^5 + (4\omega^2\zeta^2 + 2\omega^2 + 4K_PK_D)s^4 + (4\omega^3\zeta + 4K_PK_D\omega\zeta)s^3 + (\omega^4 + 4K_PK_D\omega^2\zeta^2 + 2K_PK_D\omega^2)s^2 + (K_D\omega^4 + 4K_PK_D\omega^3\zeta)s + K_PK_D\omega^4 \quad (11.b)$$

The driving requirements and methodology used to tune the proportional and derivative gains of the RWAC controller, K_P and K_D, as well as the 4th order low-pass filter applied to the rate estimate of Fig. 4, are discussed in Ref. 3. To summarize the results, the required bandwidth of the RWAC controller is $\omega_n = 2\pi \times 0.0299\ rad/s$, and its damping coefficient is $\zeta_n = 0.4138$ (dimensionless).[3] Approximating the RWAC as a one-axis, linear, continuous-time version of the block diagram shown in Fig. 4, the 2nd order characteristic polynomial of this simplified system can be solved for its roots (poles) in terms of gains K_P and K_D. The resulting equations express K_P and K_D in terms of natural frequency, ω_n , and damping coefficient, ζ_n as shown in Eqs. (12) and (13).[10]

$$K_P = \frac{\omega_n}{2\zeta} \quad (12)$$

$$K_D = 2\zeta\omega_n \quad (13)$$

The natural frequency and damping coefficient, of the 4th order low-pass filter are $\omega = 2.34048\ rad/s$ and $\zeta = 0.4000$, respectively.[3] Taking into account that the bandwidth of the RWA controller is more than 10 times lower than the center frequency of the low-pass filter, the transfer function from Eq. (11) can be simplified by ignoring the 4th order low-pass filter.[10] A low-order transfer function between $T_D(s)$ and $e_\Theta(s)$ is presented in Eq. (14).

$$\frac{e_\Theta(s)}{T_D(s)} = -\frac{1/I_{SC}}{s^2+K_Ds+K_PK_D} = -\frac{1/I_{SC}}{s^2+2\zeta_n\omega_n s+\omega_n^2} \quad (14)$$

Since the RWAC is decoupled about the spacecraft X, Y, and Z-axes, the transfer function in Eq. (14) can be used independently about each axis, only needing the spacecraft inertia, I_{SC}, to be replaced by the MOI about the specific axis of interest. Since the MEA cover actuator applies its torque vector along the ±Y-axis, only the transfer function relating $T_{D_y}(s)$ to $e_{\Theta_y}(s)$ is needed. Equation (15) presented the desired transfer function in the Laplace domain, with I_{YY} changing over time due to propellant consumption.

$$\frac{e_{\Theta_y}(s)}{T_{D_y}(s)} = -\frac{1/I_{YY}}{s^2+0.15548s+0.03529} \quad (15)$$

Applying the inverse Laplace transformation to Eq. (15) yields the approximation of the time-varying disturbance torque about the Y-axis, $T_{D_y}(t)$, as a function of Y-axis position error, $e_{\Theta_y}(t)$, and its first and second time derivatives, Y-axis rate error $\dot{e}_{\Theta_y}$, and Y-axis acceleration error, $\ddot{e}_{\Theta_y}$.

$$T_{D_y}(t) \approx -I_{YY}\left\{\ddot{e}_{\Theta_y}(t) + 0.15548\dot{e}_{\Theta_y}(t) + 0.03529e_{\Theta_y}(t)\right\} \text{ Nm} \quad (16)$$

It's important to note that the rate error, $\dot{e}_{\Theta_y}$, used in the simplified transfer function of Eq. (16) is not the same "rate error" labeled in Fig. 4. The rate error called out in the block diagram of the RWAC controller is equal to the following expression:

$$\text{RWAC Rate Error} = \omega_C(t) + e_\Theta(t)K_P - \omega_{est}(t) \quad (17)$$

Where $\omega_C(t)$ is the commanded rate, $e_\Theta(t)$ is the position error, K_P is the proportional gain, and $\omega_{est}(t)$ is the filtered rate estimate.

The Y-axis position error (attitude control error), $e_{\Theta_y}(t)$, in Eq. (16), is available from flight data at a sampling frequency of ½ Hz, or 1 sample per 2 seconds. Cubic spline interpolation is used to obtain position error samples once every second. Once position error has been interpolated to a 1-second interval, the position error data is smoothed using the same smoothing technique used to smooth the accumulated momentum data in the torque estimation method relying on RWA rate data. That is, the position error data is smoothed using weighted linear least squares and a 2nd degree polynomial model, with a span of 8% of the total number of samples in the actuation activity. Figure 10 shows the smoothed position error about the ±Y-axis.

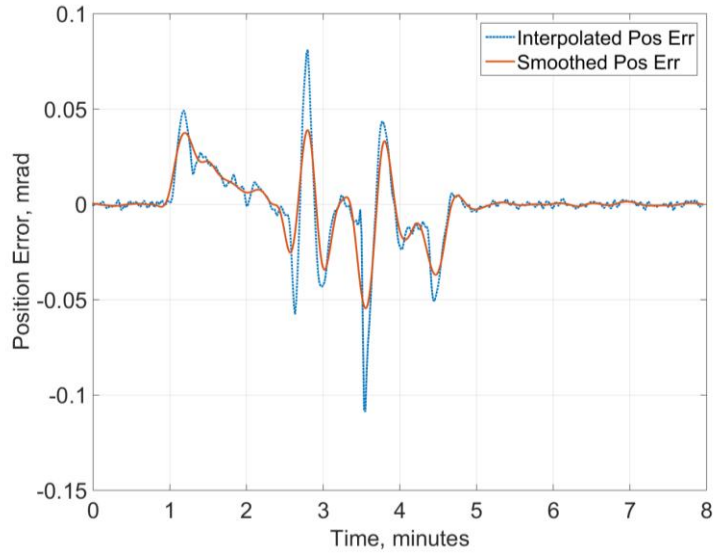

Figure 10. Smoothed Y-Axis position error. *This figure shows a comparison of the interpolated position error curves before being smoothed (blue) and after being smoothed (orange) for the deploy activity on September 29, 2015.*

Once the position error data has been smoothed, its time derivative is taken twice, as expressed in Eqs. (18) and (19).

$$\dot{e}_{\Theta_y} = \frac{de_{\Theta_y}}{dt} \approx \frac{e_{\Theta_y(i+1)} - e_{\Theta_y}(i)}{t(i+1) - t(i)} \tag{18}$$

$$\ddot{e}_{\Theta_y} = \frac{d^2 e_{\Theta_y}}{dt^2} \approx \frac{\dot{e}_{\Theta_y}(i+1) - \dot{e}_{\Theta_y}(i)}{t(i+1) - t(i)} \tag{19}$$

The smoothed position error, $e_{\Theta_y}(t)$, and its first and second time derivative given by Eqs. (18) and (19) are fed into Eq. (16), to obtain an estimate of the torque time history as given by the "transfer function" method. Consequently, the secondary method the Cassini AACS team has developed to reconstruct the disturbance torque from motor-A in the MEA cover Dual Drive Actuator (DDA) is henceforth denoted as T_{TF} and is expressed by Eq. (20).

$$T_{TF}(t) = T_{D_y}(t) \tag{20}$$

B. Results of "Transfer Function" Method of Torque Reconstruction

Figure 11 presents the torque time history obtained from the AACS transfer function method of reconstruction, which uses position error data. It is important to note that both the disturbance torque extracted from RWA momentum, $T_{H_{rwa}}$, and the disturbance torque extracted from Y-axis position error, T_{TF}, agree well in terms of the general shape of the torque profiles. Differences between the results of each method will be discussed in section IV-C, however, the author of the paper is satisfied with the agreement between the two methods, and is confident in the validity of trending the long term performance of the MEA cover actuator using the torque reconstruction method that utilizes RWA momentum.

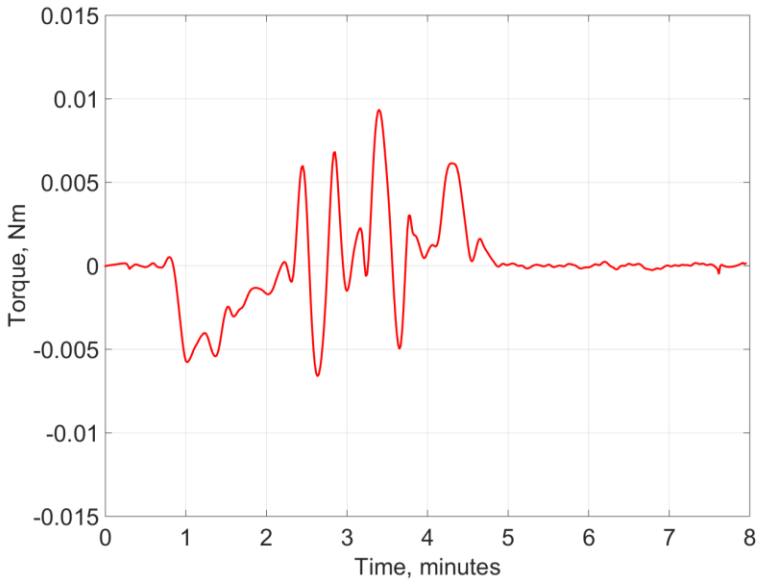

Figure 11. Disturbance torque imparted by motor-A and derived from Y-axis position error. *T_{TF} for deploy activity on September 29, 2015 shows generally good agreement with $T_{H_{rwa}}$ in Fig. 8 in terms of the torque signature being extracted.*

C. Comparison of Torques from "RWA Momentum" Reconstruction and "Transfer Function" Reconstruction

The disturbance torque time-history from motor-A in the MEA cover DDA is difficult to reconstruct, without prior knowledge of the *predicted (true)* torque time-history. However, using available flight data, the Cassini AACS team has developed two *different* methods of estimating this disturbance torque. Both methods, corroborate each other's results, but do present certain differences that must be addressed.

Figure 12 shows a comparison of both disturbance torque reconstruction methods. One observation that can be made is that the magnitude of the torque excursions in T_{TF} are significantly smaller in magnitude (~50% depending on excursion) than the corresponding torque excursions in $T_{H_{rwa}}$. The peak magnitudes of the reconstructed torque excursions in both methods are directly affected by the smoothing technique applied on the accumulated momentum about the Y-axis, H_{RWA_y}, and on the Y-axis position error, e_{θ_y}. The effects of the smoothing technique can be observed in Figs. 7 and 10. As will be discussed in section VI, the smoothing technique was tuned by adjusting the span of samples it calculates with. A span of 8% of the number of samples in a given actuation activity was chosen as the tuned value to use for this study. The 8% span causes the peak torque excursions of $T_{H_{rwa}}$ to predict the true peak torque to a smaller percent error, but causes the peak torque excursion of T_{TF} to *underestimate* the true peak torque with a much larger percent error. The decision to tune the smoothing technique to reduce percent error in $T_{H_{rwa}}$ at the expense of increasing the percent error in T_{TF} was acceptable since $T_{H_{rwa}}$ is the primary torque reconstruction method, and T_{TF} is only used as a "sanity check". The estimated percent error in $T_{H_{rwa}}$ will be discussed in section VI.

Another observation that can be made is that T_{TF} "leads" $T_{H_{rwa}}$ in time. Although the smoothing technique can contribute to the delay between the two torque profiles, because it modifies the shape of the torque excursions, another contributing factor is the natural delay between the position error registered by the spacecraft RWAC and the response of the RWAs. Although the RWAC runs through the control algorithm once every 0.125 seconds, the proportional gain, K_P, scales the commanded torque by the size of the position error (refer to RWAC block diagram in Fig. 4).[3] This means that a lag, up to 10 seconds, can be seen between the time the position error, e_{θ_y}, begins accumulating, and the time sufficient RWA rpm has been accumulated to impart a significant counteractive torque. The time lag can be observed by noticing that e_{θ_y} begins accumulating almost exactly at minute "1" (motor-A on) in Fig. 10, but RWA rate does not start steadily increasing in magnitude until a few seconds after minute "1" in Fig. 5.

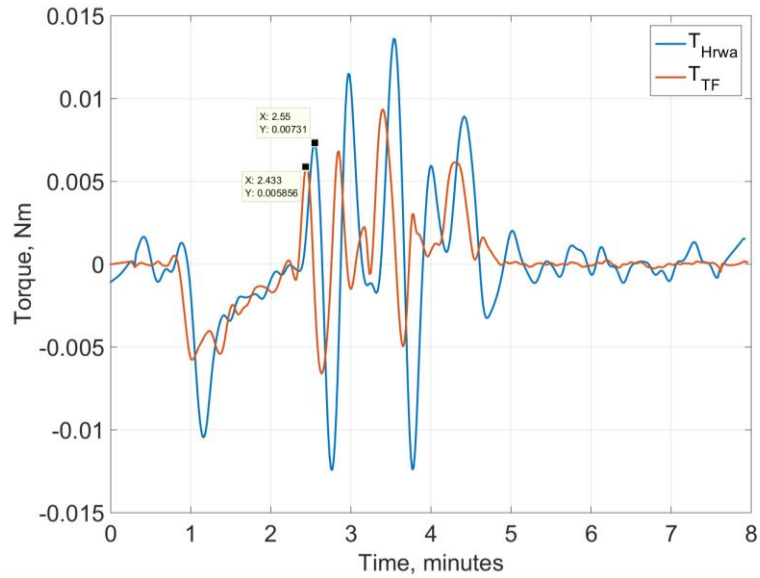

Figure 12. Comparison of motor-A imparted disturbance torque from two reconstruction methods. *This figure shows a comparison of both methods of Y-axis torque reconstruction for the MEA cover deployment that took place on September 29, 2015.*

V. Trending Analysis of Cassini MEA Cover Actuator from 2004 to 2015

The ultimate goal of this study is to find a novel method of trending the performance of the MEA cover DDA throughout its 10+ years of service on the Cassini spacecraft, using available AACS flight data. To this end, a primary torque reconstruction method has been proposed in this paper, and its results have been validated by a second torque reconstruction method. Although the DDA is composed of two motors, motor-A and motor-B, all but two cover actuations have been performed using only motor-A, while motor-B has been reserved as a backup. It is emphasized that the torque output of motor-A in the DDA cannot be directly measured because it is a torque *internal* to the Cassini system. The torque that is calculated via $T_{H_{rwa}}$ and T_{TF} is the *dynamic response* of the spacecraft to the motion of the MEA cover mechanism, called the "disturbance" torque. Any unexpected behavior in the disturbance torque trends may indirectly point to degradation in motor-A.

A. Torque Time History Trend Using "RWA Momentum" Reconstruction Method (2004-2015)

At the time of writing this paper, the Cassini MEA cover has been actuated by motor-A, in the DDA, nearly 80 full cycles (1 cycle = 1 deploy + 1 stow). For the purpose of this study, it is sufficient to analyze data from 1 deploy activity per year, from 2004 to 2015. The earliest deploy data that is analyzed in this paper is from December 9th, 2004. This deployment took place immediately before the Huygens probe was launched from the Cassini orbiter into Titan's atmosphere on December 25, 2004. From then on, no changes in the Cassini mass properties took place, besides the steady depletion of monopropellant and bipropellant supply. During the years of 2013 and 2014 there were no MEA cover actuations. After a long pause from MEA cover actuations, on July 14th, 2015 an MEA cover actuation test was conducted which deployed and stowed the cover on the same day. The first deploy activity that took place in 2015 for dust-hazard mitigation was on September 29th. The 2015 July and September actuations are also included in this paper. A complete list of the actuation dates used in this paper are presented in the Table 1. As stated previously, only deployment data will be analyzed in this paper, with stow data included in Appendix B.

Figure 13 presents the trending plot for all MEA cover deployments that were reconstructed using the RWA momentum method, that is, they represent $T_{H_{rwa}}$ from Eq. (9). The older actuations are colored in a lighter shade of grey and the tone darkens to black as the actuations become more recent. The deployment of 2004 is also marked with blue dots, to distinguish it as the only included deployment that occurred before the ejection of the Huygens probe. The most recent deployment included in this paper (September 29, 2015) is colored in red.

From visual inspection of the torque time-histories in Fig. 13, it can be said that all MEA cover deployments since 2004 to 2015 follow the same general trend in terms of placement of major torque excursions. No torque time-histories, $T_{H_{rwa}}$, exhibit any *prominent* deviation from the nominal signature of the rest of the group.

Table 1. List of MEA cover deployments used in annual trend analysis

Actuation type	Actuation date	Days since last chronological actuation	Days since last trended actuation
Deploy	9 December 2004	161	-
Deploy	9 July 2005	12	211
Deploy	19 May 2006	219	314
Deploy	28 August 2007	39	466
Deploy	30 October 2008	6	429
Deploy	13 October 2009	345	347
Deploy	28 November 2010	161	411
Deploy	10 September 2011	242	286
Deploy	12 October 2012	145	398
No MEA cover actuations took place in 2013 or 2014			
Deploy	14 July 2015	997	1004
Deploy	29 September 2015	77	442

The table above lists the deployments that were analyzed in sections *V-A and V-B*. Note that additional deployments occurred from 2004 to 2015 that were not included in the trend analysis. The column titled "Days since last chronological actuation" reports the days between consecutive actuations, regardless if the previous actuation is used in the analysis of this paper or not. The column "Days since last trended actuation" only reports the lapse between consecutive deployment activities that are used in the analysis of sections *V-A and V-B*.

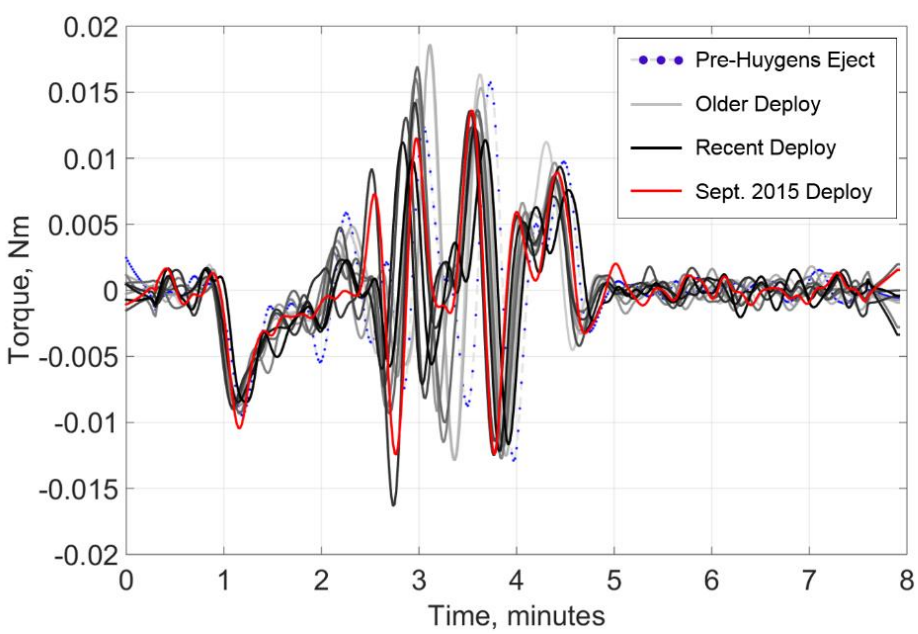

Figure 13. Trending plot of motor-A disturbance torque derived from Y-axis RWA momentum. *This figure plots $T_{H_{rwa}}$ for 11 MEA cover deployments from 2004 to 2015 (see Table 1 for list of deployments).*

B. Torque Time History Trend Using "Transfer Function" Reconstruction Method (2004-2015)

The same deployment activities from Table 1 were used to create the trending plot in Fig. 14. Figure 14 presents the trending plot for all MEA cover deployments that were reconstructed using the position error transfer function method, that is, they represent T_{TF} from Eq. (20). From visual inspection of the torque time-histories in Fig. 14, it can be said that all MEA cover deployments since 2004 to 2015 follow the same general trend in terms of placement of major torque excursions. No torque time-histories, T_{TF}, exhibit any *prominent* deviation from the nominal signature of the rest of the group.

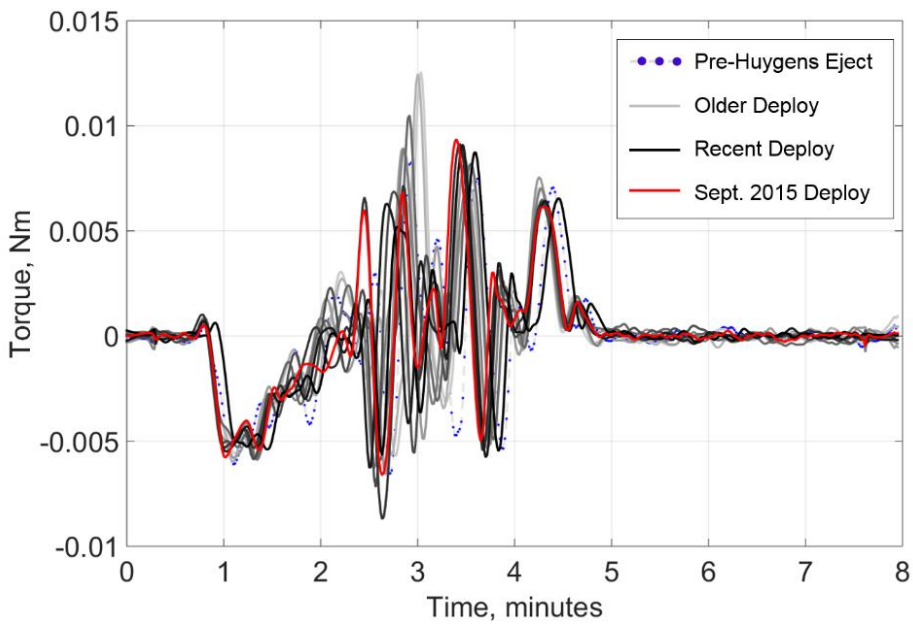

Figure 14. Trending plot of motor-A disturbance torque derived from Y-axis position error. *This figure plots T_{TF} for 11 MEA cover deployments from 2004 to 2015.*

From Figs. 13 and 14, *qualitative* observations can be made that suggest there is no troublesome trend in the torque profiles, that might signal accelerated degradation of the MEA cover DDA (motor-A). However, because of a lack of a model that explains the dynamics present in the actuation torques, and because of inherent assumptions and uncertainties in the reconstruction methods, it is difficult to extract *quantitative* insight from the trending analysis. Nevertheless, what follows is an attempt to quantify the trends present in the torque time histories.

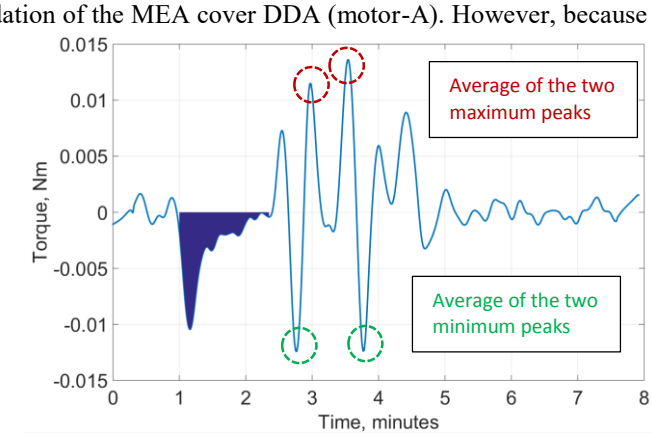

Figure 15. FOMs for motor-A torque derived from Y-axis RWA momentum. *The area under the $\boldsymbol{T_{H_{rwa}}}$ curve, from minutes "1 to 2.35" quantifies the 1st dynamics. The mean of the two max peaks and the mean of the two min peaks quantify the 2nd dynamics.*

The torque time histories in Fig. 13 and 14 indicate that motor-A induces a "negative" reaction torque in the RWAs about the Y-axis from the beginning of the actuation at minute "1" up until approximately minute "2.3", at which point a more "chaotic" torque output is observed with pronounced torque excursions that switch polarity until the torque profile begins to settle after minute "4". From this observation, it is conjectured that there at least two separate types of dynamics occurring during the MEA cover deployments, the first which govern the actuation from minute "1" to approximately minute "2.3", and the second dynamics which govern the remainder of the actuation.

To characterize the quantitative change in the dynamics that govern the beginning of the actuations, a *figure of merit* (FOM) is defined. The angular impulse between minute "1" and minute "2.35" is calculated as the area under the torque vs. time curve, and is used as a FOM to quantify the change in disturbance torque. Figures 15 and 16

illustrate how the angular impulse is computed for the MEA cover deployment that took place on September 29, 2015. Figure 17 plots the trend of impulse over the 11 deployments analyzed, using both methods of AACS torque reconstruction. It can be seen that both trends increase in magnitude of impulse at a similar rate. The increase of impulse magnitude over time may be due to increased roughness in the path the cover travels. $T_{H_{rwa}}$ impulse increases by ~30% from 2004 to 2015.

Another FOM that can be used to quantitatively trend the change in deployment torque profiles over time is the arithmetic mean of the magnitudes of the two maximum excursions and the arithmetic mean of the magnitudes of the two minimum excursions in each reconstruction, as illustrated in Figs. 15 and 16. This FOM serves to characterize the changing dynamics governing the deployments after minute "2.35", which may be dominated by the roughness that motor-A has to overcome along the deployment path. Figure 18 presents four data sets. The *blue star markers* represent the mean of the two maximum torque excursions in each deployment reconstructed from RWA momentum. The *blue circle markers* represent the mean of the two maximum torque excursions in each deployment reconstructed from position error. The *red star markers* represent the mean of the two minimum torque excursions in each deployment reconstructed from RWA momentum. The *red circle markers* represent the mean of the two minimum torque excursions in each deployment reconstructed from positon error. It's observed that both $T_{H_{rwa}}$ data sets decrease gradually in magnitude over time. $T_{H_{rwa}}$ peak excursions decrease in magnitude by ~33% from 2004-2015.

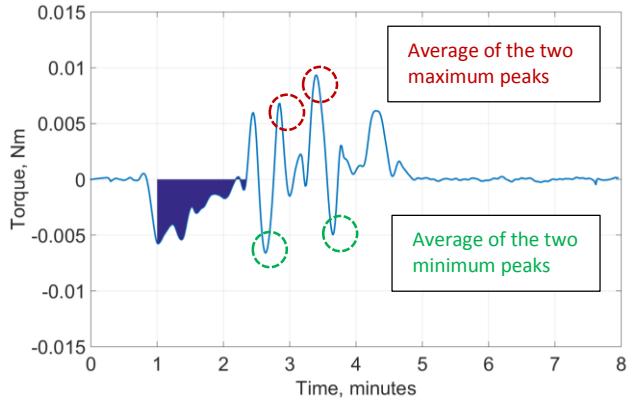

Figure 16. FOMs for motor-A torque derived from Y-axis position error. *The area under the $\boldsymbol{T_{TF}}$ curve, from minutes "1 to 2.35" quantifies the 1st dynamics. The mean of the two max peaks and the mean of the two min peaks quantify the 2nd dynamics.*

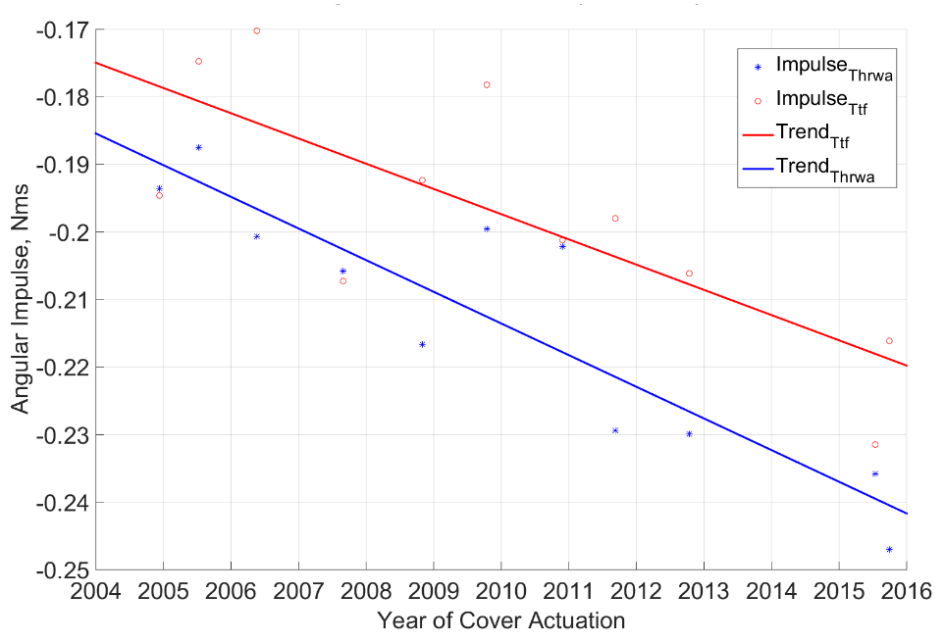

Figure 17. Angular impulse trends. *This figure presents the two impulse trends that are obtained by calculating the area under the $T_{H_{rwa}}$ and T_{TF} profiles, for the deployments listed in Table 1 from 2004 to 2015.*

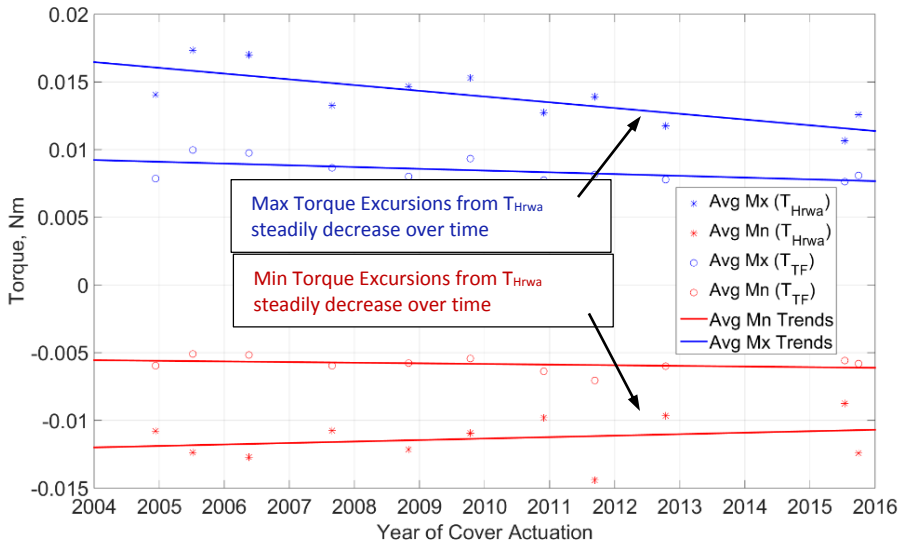

Figure 18. Peak torque excursion trends. *This figure presents the trends of the mean of the two maximum and two minimum torque excursions from reconstructed torque profiles, $T_{H_{rwa}}$ and T_{TF}. The blue star markers represent the mean of the two maximum torque excursions in each deployment reconstructed from RWA momentum. The blue circle markers represent the mean of the two maximum torque excursions in each deployment reconstructed from position error. The red star markers represent the mean of the two minimum torque excursions in each deployment reconstructed from RWA momentum. The red circle markers represent the average of the two minimum torque excursions in each deployment reconstructed from positon error. Table 1 lists the deployment activities used.*

C. Possible Variations in Torque Time History Trends After Periods of "Hibernation"

Another check that can be done to evaluate the health of the MEA cover mechanism is to compare torque profiles immediately before and after long periods of inactivity, similar to hibernation cycles in animals. Inactivity in an actuation system can cause lubrication and impingement problems that go away as the system is "warmed up" through use. Three pairs of deployments are plotted in Figs. 19 and 20. The first deployment in each pair comes immediately after a long period of time where the cover was not actuated, and is called the "cold" actuation. The second deployment in each pair is the actuation immediately after the cold actuation, and is called the "warm" actuation. Corresponding cold and warm actuations are plotted in the same shade of color, with all cold actuations denoted with an "X" marker, and all warm actuations denoted with a "O" marker. Stows cannot be used in this type of trending because they are always preceded by a deployment activity, such that all stow activities are "warm". Table 2 lists the actuations used for Figs. 19 and 20.

Table 2. List of MEA cover deployments used in post-hibernation trend analysis

Actuation type	Actuation date	Days since last chronological actuation	Hibernation State
Deploy	19 May 2006	219	"Cold"
Deploy	29 June 2006	38	"Warm"
Deploy	13 October 2009	345	"Cold"
Deploy	31 October 2009	17	"Warm"
No MEA cover actuations took place in 2013 or 2014			
Deploy	14 July 2015	997	"Cold"
Deploy	29 September 2015	77	"Warm"

The table above lists the deployments that were analyzed in section *V-C*. Note that additional deployments occurred from 2004 to 2015 that were not included in the trend analysis. The column titled "Days since last chronological actuation" reports the days between consecutive actuations, regardless if the previous actuation is used for the analysis of this paper or not. The column "Hibernation State" does not refer to the temperature of the MEA cover mechanism, but rather to its state of inactivity. "Cold" deployments occurred after a long period of inactivity, and "warm" deployments occurred after a "cold" deployment and after the follow-up stow actuation.

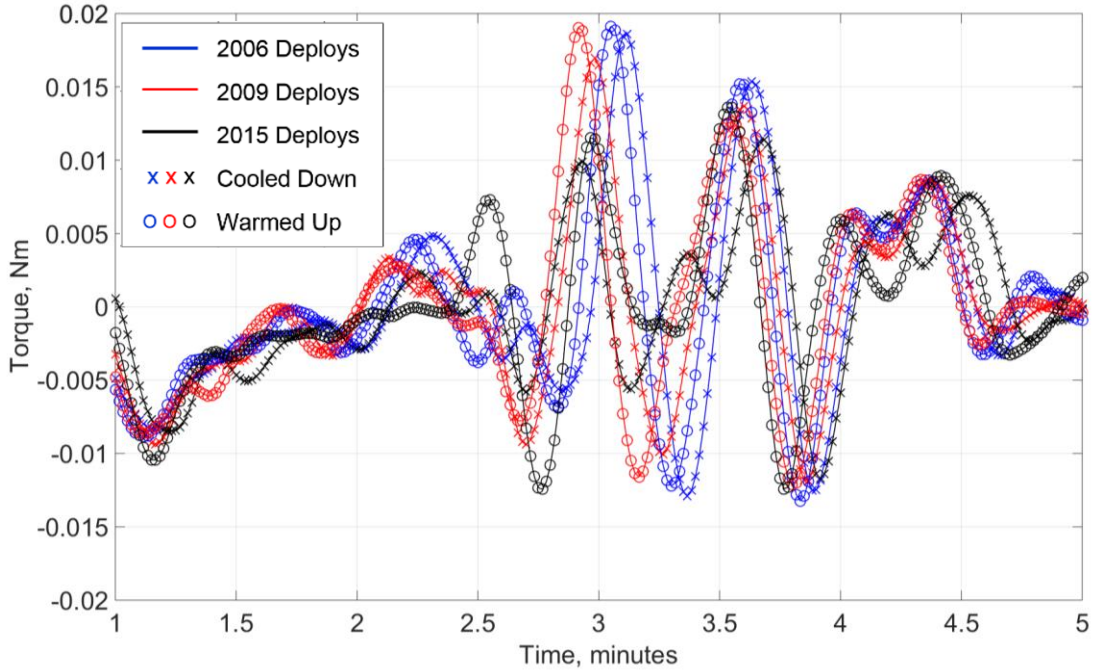

Fig 19. "Hibernation" trending using Y-axis RWA momentum data. *This figure shows $T_{H_{rwa}}$ for three pairs of deployments. Each pair is made up of one "cold" deployment which refers to a deployment immediately after a long period of MEA cover inactivity, and one "warm" deployment which refers to a deployment after the "cold" deployment and after the accompanying stow actuation. Each color corresponds to a different pair, and* X *markers indicate "cold" deployments and* O *markers indicate "warm" deployments.*

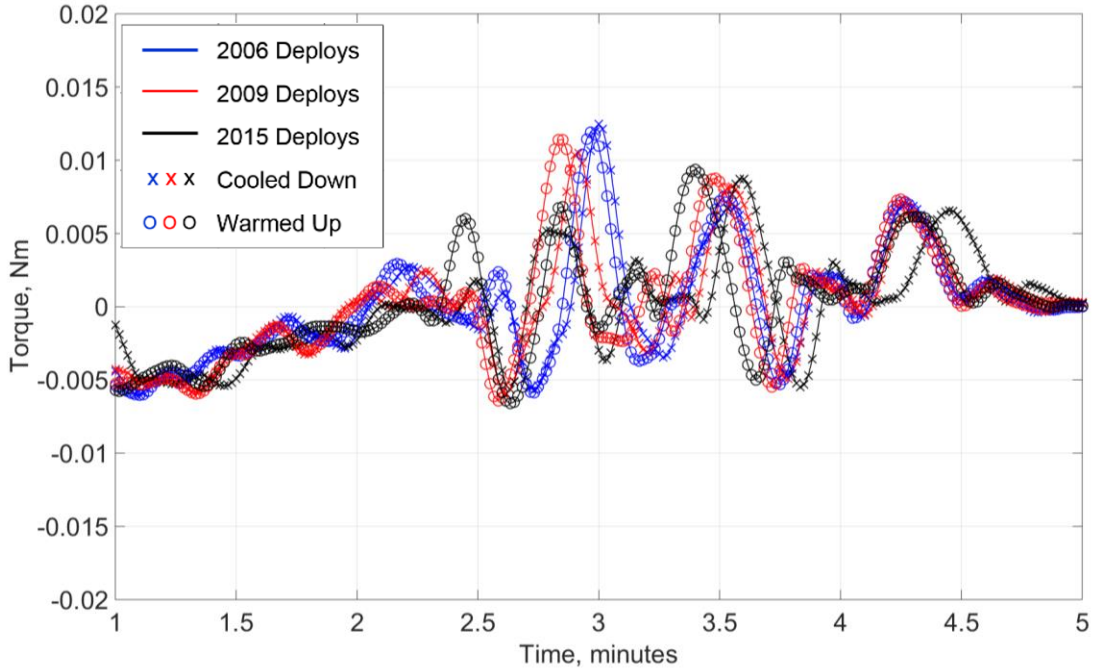

Fig 20. "Hibernation" trending using Y-axis position error data. *This figure shows T_{TF} for three pairs of deployments. Each pair is made up of one "cold" deployment which refers to a deployment immediately after a long period of MEA cover inactivity, and one "warm" deployment which refers to a deployment after the "cold" deployment and after the accompanying stow actuation. Each color corresponds to a different pair, and* X *markers indicate "cold" deployments and* O *markers indicate "warm" deployments.*

What is important to note in Figs 19 and 20 is that for the most part, the torque profiles between the "cold" and "warm" deployments are comparable in shape and in torque magnitude. This implies that long periods of inactivity cause no major effect on the performance of the MEA cover DDA.

VI. Quantitative Estimation of Percent Error in Torque Estimations

It is difficult to come up with an *analytical* uncertainty figure for the torque reconstruction methods presented in this paper, without having a description of the true dynamics governing the MEA cover actuations. Instead, what is presented in this section is an experimental method to estimate the percent error inherent to $T_{H_{rwa}}$ using the Cassini high fidelity simulation environment called Flight Software Dynamic Simulation (FSDS). FSDS is an all-software simulation environment with full environmental dynamics built in. It was originally designed for flight software (FSW) testing before launch, and has since then been adopted as a high-fidelity analysis tool. FSDS is currently used by the Cassini team to test FSW revisions, sequence verification, and delta-V estimate generation which is used by the Navigation team.[6] During real MEA cover actuations, the spacecraft is commanded to a quiescent attitude and an *unknown* reaction torque is imparted about the Y-axis as motor-A rotates the cover. FSDS allows the user to *inject* a *known* external torque profile into a simulation of the Cassini spacecraft while at a quiescent attitude. The FSW will react to the FSDS injected torque by commanding the RWAs to spin up according to the RWAC control system. The simulated FSDS RWA rates and position error is output at the same sampling rate as real flight data. The two torque reconstruction methods outlined in this paper, $T_{H_{rwa}}$ and T_{TF} , are then applied to the FSDS simulated flight data. An estimate of percent error is obtained by comparing only the $T_{H_{rwa}}$ reconstructed torque profile to the *known* injected torque profile. Percent error for T_{TF} is not calculated because it is known that the smoothing technique causes T_{TF} to underestimate the true torque magnitude.

A. Tuning the RWA Momentum and Position Error Smoothing Technique using FSDS Simulation

In addition to providing a method of estimating the percent error of $T_{H_{rwa}}$, FSDS provided a method of tuning the smoothing technique that is applied to the noisy RWA momentum used in calculating $T_{H_{rwa}}$ and the position error used in calculating T_{TF} . The smoothing technique is tuned by changing the *span* of samples it uses to calculate each new "smoothed" sample. Different external torque profiles were injected into FSDS, and different spans were tested to see which span would output the best estimate of the various injected torque profiles. Ultimately, a span of 8% of the total number of samples was settled upon, as it minimized percent error in the reconstruction of the various injected torque profiles, without overly damping the reconstructed torque excursions.

B. Percent Error Estimation for Torque Reconstruction Methods Using External Torque Profile #1

The following percent error is derived by comparing $T_{H_{rwa}}$ to an injected FSDS torque profile created by repeating a triangular pulse function with rise and fall time of 30 seconds, with alternating peak torque of ±0.0198 Nm. From Fig. 21 it is seen that T_{TF} , which is derived from position error data, does not exhibit the time lag from the true torque profile (FSDS injected torque) as $T_{H_{rwa}}$ does. It is also seen that $T_{H_{rwa}}$ more closely matches the magnitudes of the peak torque excursions of the true torque profile.

Table 3 shows the percent error calculated between $T_{H_{rwa}}$ and the true FSDS injected torque. Percent error is only calculated at the 6 peak excursions of the FSDS true torque profile. This is done to avoid invalid error estimates in torque regimes where the signal-to-noise ratio would be too low for either torque reconstruction method to provide reasonable results. Such a regime is seen between minute "0" and "1", where the true torque is zero, but both reconstruction methods predict nonzero torque.

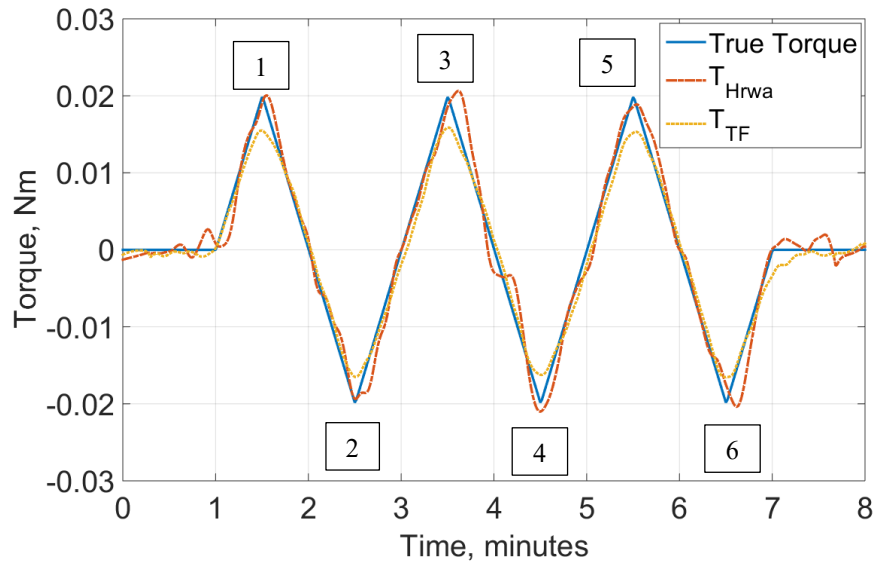

Figure 21. Comparison of reconstructed torques to FSDS injected torque profile #1. *This figure compares $T_{H_{rwa}}$ and T_{TF} against an FSDS injected triangular torque profile with rise/fall time of 30 seconds each.*

Table 3. Percent error for FSDS-injected torque profile #1

Reconstruction method	Peak Errors (%)						Max Peak Error (%)
	Peak 1	Peak 2	Peak 3	Peak 4	Peak 5	Peak 6	
$T_{H_{rwa}}$	1.20	2.38	4.08	5.97	4.74	2.81	**5.97**

The table above presents the peak percent error between $T_{H_{rwa}}$ and the true torque profile #1 that was injected into FSDS. The maximum peak error between the reconstructed torque and the true torque occurs at peak 4, and is 5.97%

C. Percent Error Estimation for Torque Reconstruction Methods Using External Torque Profile #2

The following percent error is derived by comparing $T_{H_{rwa}}$ to an injected FSDS torque profile created by repeating a triangular pulse function with rise and fall time of 15 seconds, and alternating peak torque of ±0.0197 Nm. From Fig. 22 it is seen that T_{TF} , which is derived from position error data, does not exhibit the time lag from the true torque profile (FSDS injected torque) as $T_{H_{rwa}}$ does. It is also seen that $T_{H_{rwa}}$ more closely matches the magnitudes of the peak torque excursions of the true torque profile.

Table 4 shows the percent error calculated between $T_{H_{rwa}}$ and the FSDS injected torque (profile #2) in the same manner as the percent errors in Table 3 were calculated. Taking the more conservative percent error, it is assessed that $T_{H_{rwa}}$ estimates the major excursions of the true MEA cover deployment torque profile with a percent error of ~10%.

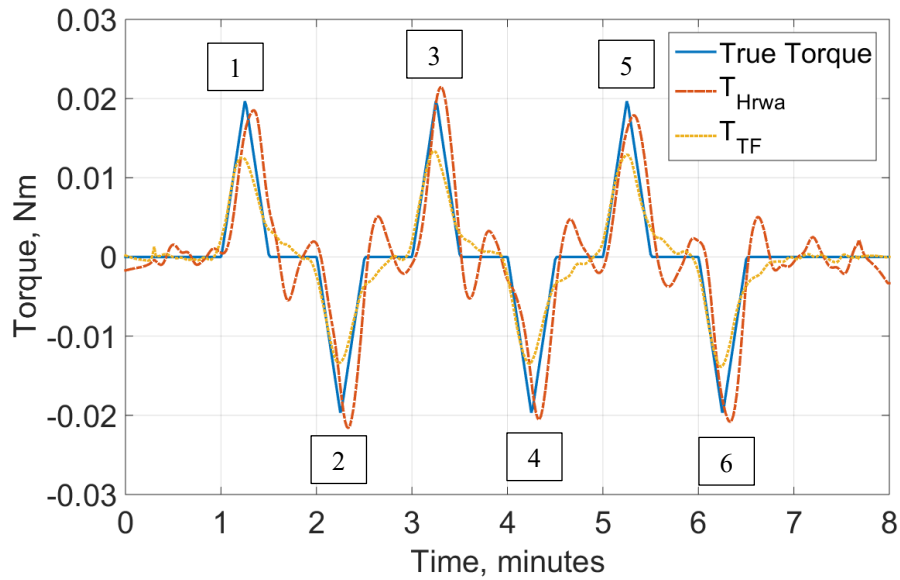

Figure 22. Comparison of reconstructed torques to FSDS injected torque profile #2. *This figure compares $T_{H_{rwa}}$ and T_{TF} against an FSDS injected triangular torque profile with rise/fall time of 15 seconds each.*

Table 4. Percent error for FSDS-injected torque profile #2

Reconstruction method	Peak Errors (%)						Max Peak Error (%)
	Peak 1	Peak 2	Peak 3	Peak 4	Peak 5	Peak 6	
$T_{H_{rwa}}$	5.87	9.91	9.11	4.38	9.13	5.89	**9.91**

The table above presents the peak percent error between $T_{H_{rwa}}$ and the true torque profile #2 that was injected into FSDS. The maximum peak error between the reconstructed torque and the true torque occurs at peak 2, and is 9.91%. Between the max peak error of Table 3, 5.97%, and that of Table 4, 9.91%, the more conservative percent error of 9.91% is taken as the percent error for the overall method of estimating $T_{H_{rwa}}$.

VII. Conclusion

This purpose of this study was to trend the performance of the Cassini MEA cover actuator mechanism (motor-A of the DDA) over the span of the mission from 2004 until 2015. The Cassini SCO team cannot directly measure motor torque output, so an indirect method of trending the performance of the MEA cover motor was developed. A method of estimating the *disturbance torque* imparted on the spacecraft during MEA cover actuations was outlined. Trending these disturbance torque profiles from 2004 to 2015 provides a way to assess the changes in the resistance or stiffness in the cover. The principle of conservation of angular momentum using spacecraft RWA rates led to an accumulated angular momentum estimate which was then used to estimate disturbance torque. The spacecraft angular momentum at the end of each cover actuation returned to its original value, demonstrating there was no "external" torque imparted by the activity – confirming that Cassini is an *isolated* system during these MEA cover actuations.

The method of torque reconstruction using RWA data was validated by a second method of torque reconstruction which used spacecraft attitude control (position) error and a "positon error to torque" transfer function. Both methods agreed well in terms of the estimated torque signature. The analysis methodology was independently checked using ground and flight software simulations. This simulation was used to estimate an upper bound of about 10% error in the disturbance torque estimate for the RWA angular momentum approach.

Both methods showed a *repeatable* trend in the reconstruction torque signatures, and more importantly, the methods reveal no sudden changes in the disturbance torque profile from one year to the next. A sudden change between reconstructed torque profiles could indicated sudden degradation or failure in the MEA cover actuator. Two figures of merit were defined to quantify an apparent gradual change in the reconstructed torque trends. The first figure

of merit is the estimated angular impulse for roughly the first 1.5 minutes of the MEA cover motion. The estimated angular impulse in this first portion of the actuation gradually increased by roughly 30% between 2004 and 2015. This gradual increase in angular impulse may be caused by internal actuator friction causing rougher cover movement, but the data is inconclusive.

The second figure of merit utilized is the mean of the two maximum torque excursion magnitudes and the mean of the two minimum torque excursion magnitudes in the latter stages of the reconstructed torque profiles. This figure of merit suggests the maximum and minimum torque excursions of the reconstructed torque profiles are gradually decreasing over time, by about 33% between 2004 and 2015. Data is inconclusive as to what these results reveal, but what is important to note is that changes in the torque profiles occur *steadily* and *gradually* over the years, indicating no anomalous behavior is present in the MEA cover mechanism. Reconstructed cover actuation torque profiles immediately after long periods of inactivity (as much as 2 to 3 years) reveal that actuator performance is not noticeably affected by this inactivity. Overall, the Cassini AACS flight data reveals some changes in the disturbance torques over 11 years at Saturn, but this is not considered anomalous behavior nor a threat to the overall health of the cover actuation mechanism.

Appendix A

Appendix A presents additional diagrams and images of the Cassini MEA cover assembly. All these diagrams and images can be found in Ref. 2.

(a) (b) 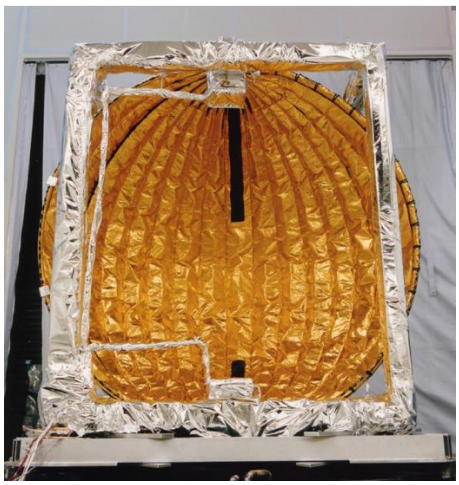

Figure A1. Engineering model of Cassini MEA cover. *This figure shows the Cassini MEA cover (a) stowed and (b) deployed while mounted to a test stand.*

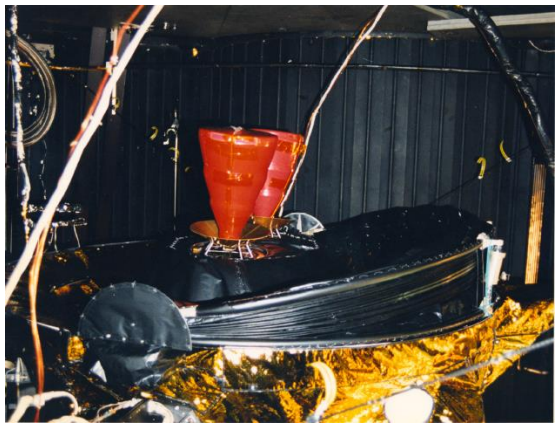

Figure A2. Flight MEA cover in stow position. *This figure shows the flight MEA cover mounted on the Cassini spacecraft in the stow position before launch.*

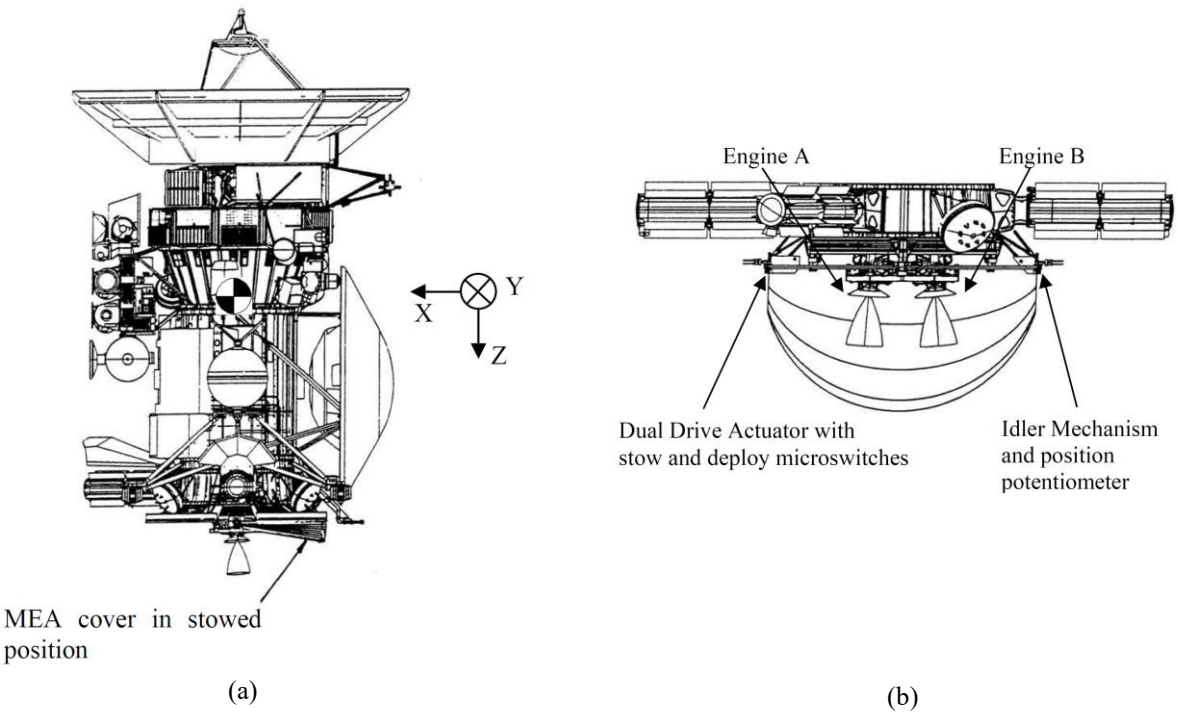

Figure A3. Cassini spacecraft layout with MEA cover. *This figure shows (a) the overall layout of the Cassini spacecraft with the MEA cover in stowed position and (b) a zoomed in view of the bottom portion of the spacecraft with the locations of the DDA and potentiometer along the cover's axis of rotation.*

Appendix B

Appendix B presents brief results of the trend analysis as it was applied to a selection of MEA cover stow activities.

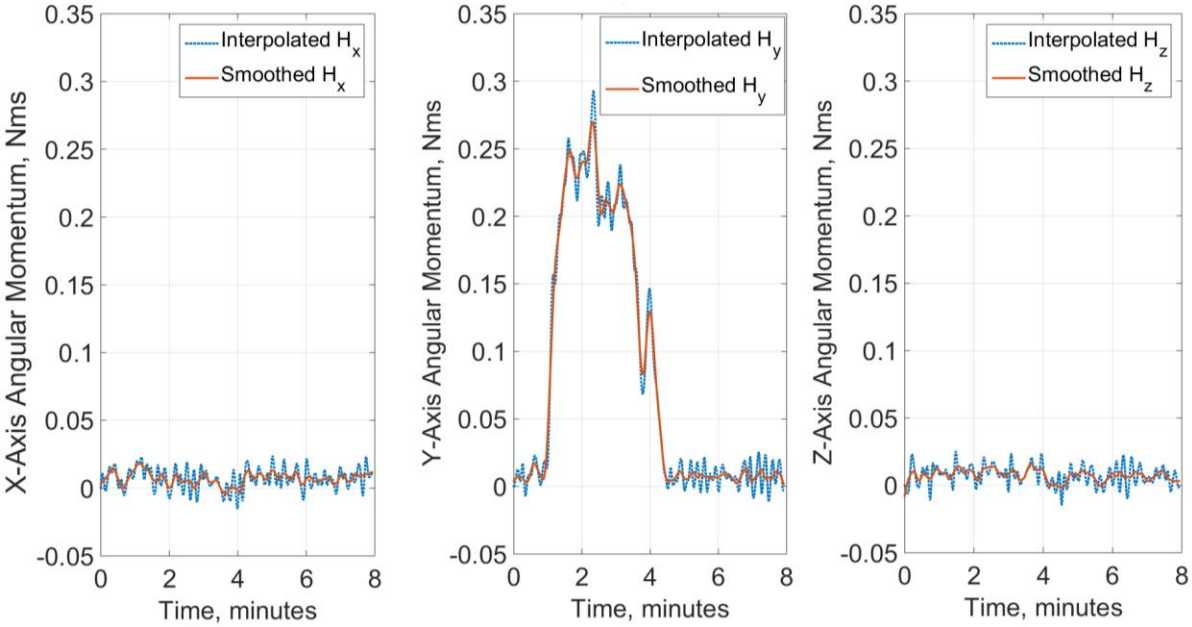

Figure B1. Smoothed Accumulated Angular Momentum from stow activity. *This figure shows a comparison of the interpolated angular momentum curves before being smoothed (blue) and after being smoothed (orange) for the MEA cover stow activity on September 30, 2015. The resulting momentum is expressed in the spacecraft body frame.*

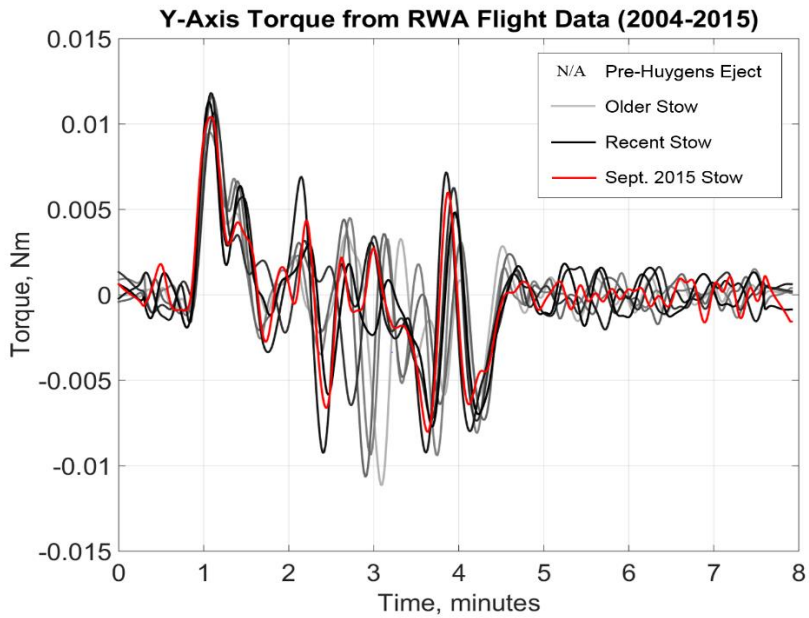

Figure B2. MEA cover stow disturbance torque derived from Y-axis RWA momentum. *This figure plots $T_{H_{rwa}}$ for 7 MEA cover stow actuations from 2006 to 2015. Refer to Table B1 for the list of plotted stow activities.*

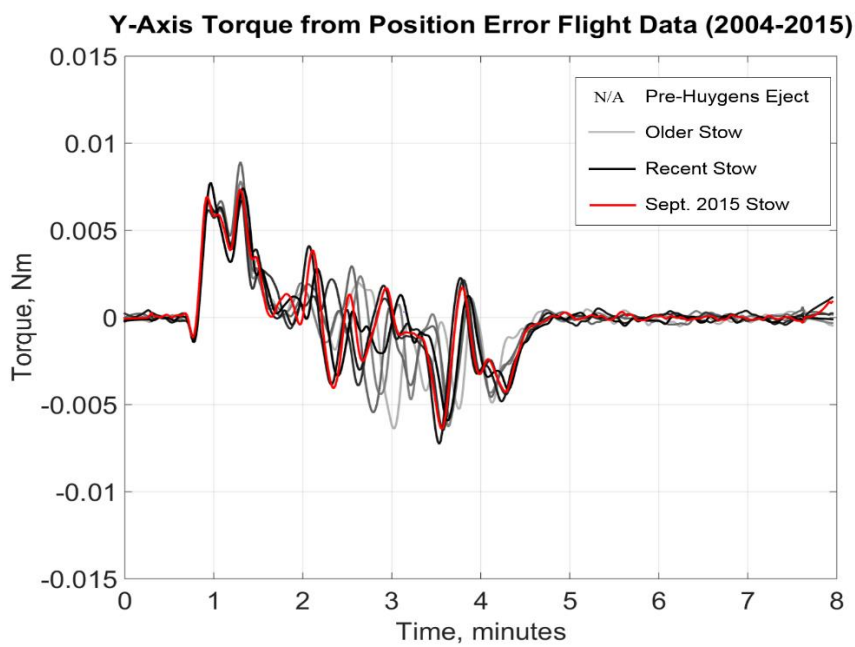

Figure 13. MEA cover stow disturbance torque derived from Y-axis attitude control error. *This figure plots T_{TF} for 7 MEA cover stow actuations from 2006 to 2015. Refer to Table B1 for a list of plotted stow activities.*

Table B1. List of MEA cover stows used in trend analysis

Actuation type	Actuation date	Days since last chronological actuation	Days since last trended actuation
Stow	22 May 2006	3	-
Stow	1 November 2008	2	894
Stow	14 October 2009	1	346
Stow	14 September 2011	4	700
Stow	19 October 2012	7	401
No MEA cover actuations took place in 2013 or 2014			
Stow	14 July 2015	0	997
Stow	30 September 2015	1	78

The table above presents the list of stows that were analyzed in the process of completing this study, but are included only in Appendix B. Note that additional stows occurred from 2006 to 2015 that were not included in the trend analysis. The column titled "Days since last chronological actuation" reports the days between consecutive actuations, regardless if the previous actuation was one of the actuations chosen for the analysis of this appendix or not. The column "Days since last trended actuation" only reports the lapse between consecutive deployment activities that are used in the analysis included in this appendix.

Acknowledgments

The work described in this paper was carried out by the Jet Propulsion Laboratory, California Institute of Technology, under contract with the National Aeronautics and Space Administration. Reference to any specific commercial product, process, or service by trade name, trademark, manufacturer, or otherwise, does not constitute or imply its endorsement by the United States Government or the Jet Propulsion Laboratory, California Institute of Technology. I wish to thank Dr. Allan Y. Lee of the Guidance and Control Section of JPL and Benjamin Marshall of the Cassini Thermal/Devices team for their critical advisement throughout this study. I also wish to thank Thomas Burk, David Bates, Todd Brown, and Eric Wang of the Cassini AACS team for their review and advisement of this study. Any remaining errors of fact or interpretation are of course the responsibility of the author.

References

[1]Burk, T.A., "Cassini at Saturn Proximal Orbits – Attitude Control Challenges," Paper AIAA-2013-4710, Proceedings of the AIAA Guidance, Navigation, and Control Conference and Exhibit, August 19-22, 2013, Boston, MA.

[2]Somawardhana, R. P., and Millard, J. M., "Cassini Main Engine Assembly Cover Flight Management and Performance", IEEEAC Paper#1075, Version 3, Aerospace Conference, 2010 IEEE, 6-13 March 2010, Big Sky, MT, 2010.

[3]Macala, G. A., "Design of the Reaction Wheel Attitude Control System for the Cassini Spacecraft," Paper AAS 02-121, AAS/AIAA Space Flight Mechanics Meeting, San Antonio, Texas, January 27–30, 2002.

[4]Lee, A. Y., and Hanover, G., "Cassini Attitude Control System Flight Performance," Proceedings of the AIAA Guidance, Navigation, and Control Conference and Exhibit, AIAA Paper 2005-6569, 2005.

[5]Sarani, Siamak, "Titan Atmospheric Density Reconstruction Using Cassini Guidance, Navigation, and Control Data", Paper AIAA-2009-5763, Proceedings of the AIAA Guidance, Navigation, and Control Conference and Exhibit, August 10-13, 2009, Chicago, Illinois.

[6]Andrade, L. G., Jr., Burk, T. A., and Pelletier, F., "Titan Density Reconstruction Using Radiometric and Cassini Attitude Control Flight Data", Paper AIAA-2015-0079, Proceedings of the AIAA Guidance, Navigation, and Control Conference and Exhibit, January 5-9, 2015, Kissimmee, Florida.

[7]Sevilla, D. R., "The Cassini Main Engine Assembly Cover Mechanism", Proceedings, 31st Aerospace Mechanisms Symposium, held at NASA Marshall Space Flight Center, May 14-16, 1997; NASA NP0-20156.

[8]Lilienthal, G. W., Olivera, A. M., and Shiraishi, L. R., "Pointing Mechanisms for the Shuttle Radar Laboratory", Proceedings, 27th Aerospace Mechanisms Symposium held at NASA Ames Research Center, May 12-14, 1993; NASA CP-3205.

[9]Packard, D. T., "Dual Drive Actuators", Proceedings, 16th Aerospace Mechanisms Symposium, held at NASA Kennedy Space Center, May 13-14, 1982; NASA CP-2221.

[10]Wang, E. K., and Lee, A. Y., "Estimation of Enceladus Plume Density Using Cassini Flight Data", Paper AIAA-2011-6551, AIAA Guidance, Navigation, and Control Conference; 8-12 Aug. 2011; Portland, OR; United States.

[11]Lee, A. Y., Wang, E. K., Pilinski, E. B., Macala, G. A., and Feldman, A. W., "Estimation and Modeling of Enceladus Plume Jet Density Using Cassini Flight Data", Journal of Spacecraft and Rockets, Vol. 50, No.2, March-April 2013.